JACS
JOURNAL OF THE AMERICAN CHEMICAL SOCIETY
Article
pubs.acs.org/JACS

Completing the Series of +2 Ions for the Lanthanide Elements: Synthesis of Molecular Complexes of Pr^{2+}, Gd^{2+}, Tb^{2+}, and Lu^{2+}

Matthew R. MacDonald, Jefferson E. Bates, Joseph W. Ziller, Filipp Furche,* and William J. Evans*

Department of Chemistry, University of California, Irvine, California 92697-2025, United States

Supporting Information

ABSTRACT: The first examples of crystallographically characterizable complexes of Tb^{2+}, Pr^{2+}, Gd^{2+}, and Lu^{2+} have been isolated, which demonstrate that Ln^{2+} ions are accessible in soluble molecules for all of the lanthanides except radioactive promethium. The first molecular Tb^{2+} complexes have been obtained from the reaction of Cp'_3Ln (Cp' = $C_5H_4SiMe_3$, Ln = rare earth) with potassium in the presence of 18-crown-6 in Et_2O at −35 °C under argon: [(18-crown-6)K][Cp'_3Tb], {[(18-crown-6)K][Cp'_3Tb]}$_n$, and {[K(18-crown-6)]$_2$(μ-Cp')}{Cp'_3Tb}. The first complex is analogous to previously isolated Y^{2+}, Ho^{2+}, and Er^{2+} complexes, the second complex shows an isomeric structural form of these Ln^{2+} complexes, and the third complex shows that $[(18\text{-crown-6})K]^{1+}$ alone is not the only cation that will stabilize these reactive Ln^{2+} species, a result that led to further exploration of cation variants. With 2.2.2-cryptand in place of 18-crown-6 in the Cp'_3Ln/K reaction, a more stable complex of Tb^{2+} was produced as well as more stable Y^{2+}, Ho^{2+}, and Er^{2+} analogs: [K(2.2.2-cryptand)][Cp'_3Ln]. Exploration of this 2.2.2-cryptand-based reaction with the remaining lanthanides for which Ln^{2+} had not been observed in molecular species provided crystalline Pr^{2+}, Gd^{2+}, and Lu^{2+} complexes. These Ln^{2+} complexes, [K(2.2.2-cryptand)][Cp'_3Ln] (Ln = Y, Pr, Gd, Tb, Ho, Er, Lu), all have similar UV−vis spectra and exhibit Ln−C(Cp') bond distances that are ∼0.03 Å longer than those in the Ln^{3+} precursors, Cp'_3Ln. These data, as well as density functional theory calculations and EPR spectra, suggest that a $4f^n5d^1$ description of the electron configuration in these Ln^{2+} ions is more appropriate than $4f^{n+1}$.

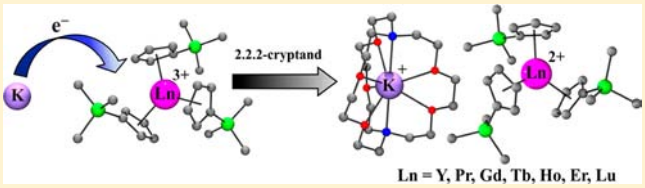

INTRODUCTION

Recently, the first crystalline examples of molecular complexes of the Y^{2+}, Ho^{2+}, and Er^{2+} ions[1,2] were obtained by potassium reduction of Cp'_3Ln, **1**, (Cp' = $C_5H_4SiMe_3$; Ln = Y, Ho, Er) in the presence of 18-crown-6, eq 1. The formation of these

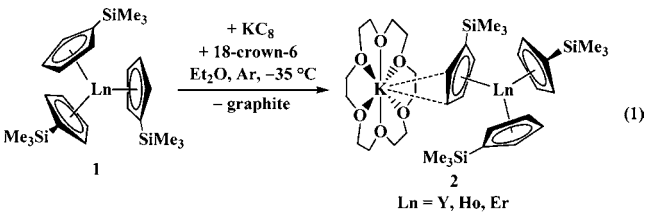

(1)

products, [(18-crown-6)K][Cp'_3Ln], **2**, raised the possibility that molecular complexes of Ln^{2+} ions could be isolated for all the lanthanide metals. Experiments to realize that goal are reported here.

Traditionally, Eu^{2+}, Yb^{2+}, Sm^{2+}, Tm^{2+}, Dy^{2+}, and Nd^{2+} were the only ions in the +2 oxidation state thought to be isolable in molecular species in the lanthanide series.[3,4] This was expected on the basis of calculated generic Ln^{3+}/Ln^{2+} reduction potentials for $4f^n/4f^{n+1}$ species[5] and data on solid-state Ln^{2+} compounds.[6−8] Specifically, since Tm^{2+}, Dy^{2+}, and Nd^{2+} are already sufficiently reducing that their complexes are unstable in ethereal solvents like Et_2O and THF,[9−18] and the other lanthanides have more negative reduction potentials, Table 1, it was thought that Ln^{2+} ions beyond Nd^{2+} in the table would be too unstable in common solvents to isolate. Furthermore, solid-state data on lanthanide dihalides, such as LnI_2, showed that only with Ln = Eu, Yb, Sm, Tm, Dy, and Nd were these species conventional $Ln^{2+}(X^{1-})_2$ salts. For all the other lanthanides, the LnX_2 solids were best described as $Ln^{3+}(X^{1-})_2(e^{1-})$ materials with a delocalized electron in a conduction band.[3,4,8,20] This meant that Ln^{2+} complexes were not accessible with these metals even under the extreme conditions of high temperature, solid-state Ln/LnX_3 reactions with the strongly reducing elemental lanthanide metals as the reductants.

Table 1. Calculated Ln^{3+}/Ln^{2+} Reduction Potentials of Yttrium and the Lanthanides[5,19]

Ln	potential (V vs NHE)	Ln	potential (V vs NHE)
Eu	−0.35	Y	−2.8
Yb	−1.15	Pr	−2.9
Sm	−1.55	Ho	−2.9
Tm	−2.3	Er	−3.1
Dy	−2.5	La	−3.1
Nd	−2.6	Ce	−3.2
Pm	−2.7	Tb	−3.7
Lu	−2.7	Gd	−3.9

Received: April 15, 2013
Published: May 22, 2013

   dx.doi.org/10.1021/ja403753j | J. Am. Chem. Soc. 2013, 135, 9857−9868

Hence, it was assumed that for La, Ce, Pr, Gd, Tb, Ho, Er, and Lu, the Ln^{2+} ions would only be observable transiently under special conditions. These ions have been identified in gas phase atomic spectra,[21,22] in ion cyclotron resonance reactivity studies,[23−25] in spectroscopic studies of Ln^{3+} ions doped into CaF_2 and irradiated with γ radiation,[26] and in electrochemical experiments in molten salts[19,27,28] and THF.[29] These studies supported the idea that these ions would be too reactive to isolate in molecules.

However, evidence for "LnA_2"-like reactivity was found for all the lanthanides through dinitrogen reduction studies. Reduction of N_2 to $(N{=}N)^{2-}$ with the traditional Ln^{2+} ions led to an LnA_3/M reaction system (A_3 = homo- or heteroleptic set of three monoanionic ligands, M = alkali metal) that generated $(N{=}N)^{2-}$ products with all other lanthanides even if a molecular Ln^{2+} ion was not known, eq 2.[1,18,30−41] Although these reactions provided evidence of Ln^{2+} reactivity, they were too complicated to provide definitive data on Ln^{2+} complexes.

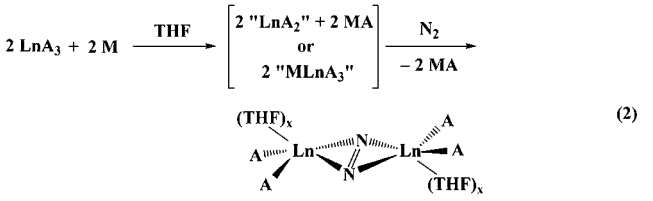

(2)

Ln = Sc, Y, La, Ce, Pr, Nd, Gd, Tb, Dy, Ho, Er, Tm, Lu
A = $N(SiMe_3)_2$, $OC_6H_3{}^tBu_2$-2,6, C_5Me_5, C_5Me_4H, $C_5H_4SiMe_3$, $C_5H_2{}^tBu_3$, BPh_4, I, H
M = K, KC_8, Na; x = 0-2

Lappert and co-workers discovered that low-valent lanthanum was also accessible in molecular form[42] and provided the first unambiguous crystallographic evidence for two more Ln^{2+} ions with molecular La^{2+} and Ce^{2+} complexes containing the $[Cp''_3Ln]^{1-}$ anion ($Cp'' = C_5H_3(SiMe_3)_2$-1,3; Ln = La, Ce), eq 3.[43] La^{2+} was identified as a $5d^1$ ion in this system, and the

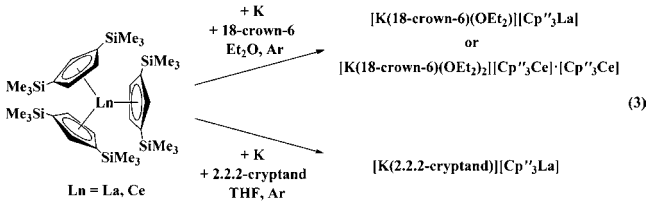

(3)

existence of these species was rationalized by noting that the 5d orbitals are close in energy to the 4f levels at the beginning of the lanthanide series.[21,44] Similar arguments could not be made for the Ho^{2+} and Er^{2+} ions made via eq 1 since holmium and erbium are late lanthanides. However, both density functional theory and UV−vis spectra suggested that the Ho^{2+} and Er^{2+} ions in complexes of **2** had $4f^n5d^1$ configurations and not the $4f^{n+1}$ configurations found for the traditional Ln^{2+} ions.[2]

If Ho^{2+} and Er^{2+} could exist in molecular complexes, it seemed that other Ln^{2+} ions should be possible. However, the Ho^{2+} and Er^{2+} complexes in eq 1 could only be isolated in Et_2O at −35 °C. Since the calculated Ln^{3+}/Ln^{2+} reduction potentials for Tb and Gd were significantly more negative than those of Ho, Er, La, and Ce, complexes of Tb^{2+} and Gd^{2+} were expected to be much less stable. In addition, it was uncertain if K (−2.9 V vs NHE) could even effect these reductions considering the calculated reduction potentials in Table 1. We now report that attempts to push the limits of Ln^{2+} chemistry to terbium via eq 1 provided insight on how to stabilize the new Ln^{2+} complexes. This has now allowed extension of +2 oxidation state chemistry across the lanthanide series.

EXPERIMENTAL SECTION

The syntheses and manipulations described below were conducted under argon with rigorous exclusion of air and water using glovebox, vacuum line, and Schlenk techniques. Solvents were sparged with UHP grade argon (Airgas) and passed through columns containing Q-5 and molecular sieves before use. NMR solvents (Cambridge Isotope Laboratories) were dried over NaK/benzophenone, degassed by three freeze−pump−thaw cycles, and vacuum transferred before use. Anhydrous $LnCl_3$ (Ln = Y, Pr, Gd, Tb, Ho, Er, Lu),[45] KCp′ (Cp′ = $C_5H_4SiMe_3$),[46] KC_8,[47] and Cp'_3Ln (Ln = Y,[1] Ho,[2] Er,[2] Lu[46]) were prepared according to the literature. 18-Crown-6 (Aldrich) was sublimed before use and 2.2.2-cryptand (4,7,13,16,21,24-hexaoxa-1,10-diazabicyclo[8.8.8]hexacosane, Aldrich) was placed under vacuum (10^{-3} Torr) for 12 h before use. Potassium mirrors were deposited by melting K under vacuum (10^{-3} Torr). ^1H NMR (500 MHz) and ^{13}C NMR (125 MHz) spectra were obtained on a Bruker GN500 or CRYO500 MHz spectrometer at 298 K. For some paramagnetic compounds, ^1H NMR spectra could only be observed when a capillary tube containing pure deuterated solvent was placed in the paramagnetic solution to assist in properly locking and shimming the instrument. IR samples were prepared as KBr pellets, and the spectra were obtained on a Varian 1000 FT-IR spectrometer. Elemental analyses were performed on a Perkin-Elmer 2400 Series II CHNS elemental analyzer. UV−vis spectra were collected in THF at 298 K using a Varian Cary 50 Scan UV−vis spectrophotometer. Kinetics experiments were conducted by quickly dissolving 30−35 mg of the analyte in 10.00 mL THF (~3 mM), transferring the solution into a quartz cuvette (1 mm path length) equipped with a greaseless stopcock, and immediately cooling the sample to −35 °C until measurement, at which time the sample was quickly warmed to room temperature in a water bath and the UV−vis spectrum collected at 298 K at intervals of 15 min for complexes of **4** and 2 min for complexes of **2**. The absorbance at λ_{max} was used to monitor changes in concentrations over time, and the plotted data are averages from several runs, with error bars depicting $\pm 3\sigma$. EPR spectra were collected using X-band frequency (9.3−9.8 GHz) on a Bruker EMX spectrometer equipped with an ER041XG microwave bridge, and the magnetic field was calibrated with DPPH ($g = 2.0036$). EPR simulations were performed as least-squares fits of the experimental spectra using the SpinCount software package[48] employing second-order perturbation in cases where hyperfine coupling was on the same order of magnitude as the Zeeman energy.

Cp'_3Pr, 1-Pr. In an argon-filled glovebox, a sealable 100 mL side arm Schlenk flask equipped with a greaseless stopcock was charged with $PrCl_3$ (452 mg, 1.83 mmol), a magnetic stirbar, and Et_2O (20 mL). A solution of KCp′ (1.00 g, 5.67 mmol) in Et_2O (20 mL) was added to the stirred slurry, and the mixture was stirred at room temperature for 12 h. The solvent was removed under vacuum from the resulting yellow-green mixture. Hexane (40 mL) was added to the reaction flask, the flask was attached to a Schlenk line, and the mixture was heated to reflux for 6 h. The solvent was removed under vacuum, and the flask was brought into a glovebox free of coordinating solvents. Additional hexane (30 mL) was added, and the resulting yellow-green suspension was filtered to remove white solids, presumably KCl and excess KCp′. The solvent was removed from the filtrate under vacuum. The resulting yellow-green solids were extracted with pentane (10 mL), and removal of solvent under vacuum afforded **1-Pr** as a microcrystalline yellow-green solid (931 mg, 92%). Yellow-green single crystals of **1-Pr** suitable for X-ray diffraction were grown from pentane at −35 °C. ^1H NMR (C_6D_6): δ 53.19 (s, $C_5H_4SiMe_3$, 6H), 4.04 (s, $C_5H_4SiMe_3$, 6H), −23.69 (s, $C_5H_4SiMe_3$, 27H). ^{13}C NMR (C_6D_6): δ 296.4 ($C_5H_4SiMe_3$), 278.4 ($C_5H_4SiMe_3$), 264.4 ($C_5H_4SiMe_3$), −28.3 ($C_5H_4SiMe_3$). IR: 3127w, 3102w, 3060w, 2953m, 2895m, 2714w, 2463w, 2232w, 2077w, 1995w, 1931w, 1871w, 1741w, 1648w, 1546w, 1442m, 1411m, 1363m, 1312m, 1243s, 1195m, 1177s, 1059m, 1041s, 985w, 902s, 832s, 771s, 750s,

dx.doi.org/10.1021/ja403753j | J. Am. Chem. Soc. 2013, 135, 9857−9868

685m, 630m cm^{-1}. Anal. calcd for $C_{24}H_{39}Si_3Pr$: C, 52.15; H, 7.11. Found: C, 51.69; H, 7.43.

Cp'_3Gd, 1-Gd. As described for **1-Pr**, $GdCl_3$ (294 mg, 1.12 mmol) and KCp′ (600 mg, 3.40 mmol) were combined to produce **1-Gd** as a microcrystalline bright-yellow solid (579 mg, 91%). Bright-yellow single crystals of **1-Gd** suitable for X-ray diffraction were grown from pentane at −35 °C. ^{1}H NMR (C_6D_6): δ 1.24 (s, $C_5H_4SiMe_3$, 6H), 0.87 (s, $C_5H_4SiMe_3$, 6H), −0.33 (br s, $\nu_{1/2}$ = 1560 Hz, $C_5H_4Si\mathit{Me}_3$, 27H). Due to the overlap of the broad Cp′ resonances, accurate peak integrations could not be obtained and are therefore approximate. IR: 3066w, 2952m, 2895m, 2714w, 2669w, 2616w, 2420w, 2364w, 2342w, 2231w, 2078w, 1997w, 1933w, 1872w, 1774w, 1749w, 1654w, 1550w, 1441s, 1414m, 1400m, 1364s, 1312m, 1243s, 1196m, 1177s, 1061s, 1041s, 903s, 832s, 774s, 751s, 685s, 630s cm^{-1}. Anal. calcd for $C_{24}H_{39}Si_3Gd$: C, 50.65; H, 6.91. Found: C, 50.50; H, 6.92.

Cp'_3Tb, 1-Tb. As described for **1-Pr**, $TbCl_3$ (296 mg, 1.12 mmol) and KCp′ (600 mg, 3.40 mmol) were combined to produce **1-Tb** as a microcrystalline bright-yellow solid (556 mg, 87%). Bright-yellow single crystals of **1-Tb** suitable for X-ray diffraction were grown from pentane at −35 °C. ^{1}H NMR (C_6D_6): δ 464.6 (br s, $\nu_{1/2}$ = 1185 Hz, $C_5H_4SiMe_3$, 6H), 125.6 (br s, $\nu_{1/2}$ = 1180 Hz, $C_5H_4SiMe_3$, 6H), −151.3 (s, $C_5H_4Si\mathit{Me}_3$, 27H). IR: 3075w, 2953w, 2894w, 2716w, 2460w, 2388w, 2232w, 2128w, 2047w, 1999w, 1934w, 1875w, 1752w, 1654w, 1442m, 1414m, 1400m, 1365m, 1312m, 1243s, 1197m, 1178s, 1062m, 1041s, 904s, 886m, 834s, 774s, 752s, 686m, 631m cm^{-1}. Anal. calcd for $C_{24}H_{39}Si_3Tb$: C, 50.51; H, 6.89. Found: C, 50.63; H, 7.23.

[(18-crown-6)K][Cp'_3Tb], 2-Tb. In an argon-filled glovebox, Cp'_3Tb, **1-Tb** (380 mg, 0.666 mmol), and 18-crown-6 (176 mg, 0.666 mmol) were combined, dissolved in Et_2O (6 mL), and cooled to −35 °C in the freezer. This solution was passed through a prechilled flash reduction column packed with excess KC_8 as previously described.[2] The dark-maroon-brown filtrate was stored at −35 °C for 12 h. The purple-brown mother liquor was decanted, and the resulting black crystalline solids were rinsed with cold 1:1 Et_2O/pentane (5 mL, −35 °C) and dried under vacuum to yield **2-Tb** as a black/maroon-brown crystalline solid (179 mg, 31%). Large single crystals of **2-Tb** suitable for X-ray diffraction were obtained by reacting a concentrated Et_2O solution of **1-Tb** and 18-crown-6 with K mirror overnight at −35 °C without stirring. IR: 3082m, 3065w, 2949m, 2886s, 2828m, 2797w, 2746w, 1977w, 1593w, 1471m, 1452m, 1436m, 1401m, 1352s, 1285m, 1237m, 1175s, 1110s, 1037m, 961m, 904m, 832s, 769m, 751m, 682w, 628m cm^{-1}. Anal. calcd for $C_{36}H_{63}O_6Si_3KTb$: C, 49.46; H, 7.26. Found: C, 49.47; H, 7.14. UV−vis (Et_2O) λ_{max}, nm (ε, M^{-1} cm^{-1}): 291 (6000), 446 (2800), 650 (1000 shoulder).

{[(18-crown-6)K][Cp'_3Tb]}$_n$, 2-Tb′. In a manner similar to that described for **2-Tb**, a solution of Cp'_3Tb, **1-Tb** (184 mg, 0.323 mmol), 18-crown-6 (93 mg, 0.35 mmol), and KCp′ (14 mg, 0.079 mmol) in Et_2O (4 mL) was chilled to −35 °C and quickly passed through a glass column packed with excess KC_8. The resulting dark-maroon-brown filtrate was stored at −35 °C for 3 weeks and deposited black/maroon-brown X-ray quality crystals of **2-Tb**′·$^1/_2$(18-crown-6)·$^1/_2$(Et_2O) (66 mg, 20%). IR: 3082m, 3065w, 2948m, 2886s, 2828m, 2797m, 2746w, 1976w, 1594w, 1471m, 1452m, 1436m, 1403w, 1352s, 1285m, 1237s, 1175s, 1109s, 1037s, 961s, 904m, 831s, 769m, 751s, 729m, 682m, 627m cm^{-1}. Anal. calcd for $C_{36}H_{63}O_6Si_3KTb$·$^1/_2$($C_{12}H_{24}O_6$): C, 50.13; H, 7.51. Found: C, 49.87; H, 7.49.

{[(18-crown-6)K]$_2$(μ-Cp′)}{Cp'_3Tb}, 3-Tb. In an argon-filled glovebox, a solution of Cp'_3Tb, **1-Tb** (157 mg, 0.275 mmol), and 18-crown-6 (73 mg, 0.28 mmol) in Et_2O (4 mL) was chilled to −35 °C and transferred to a scintillation vial containing a K mirror (15 mg, 3.8 mmol). After storing the vial at −35 °C for 3 d without agitation, black/maroon-brown single crystals began to deposit. These crystals were analyzed by X-ray diffraction and determined to be **3-Tb**·1.5(Et_2O) (30 mg, 8%).

[K(2.2.2-cryptand)][Cp'_3Y], 4-Y. In an argon-filled glovebox, Cp'_3Y, **1-Y** (252 mg, 0.503 mmol), and 2.2.2-cryptand (189 mg, 0.503 mmol) were combined and dissolved in THF (2 mL). KC_8 (88 mg, 0.65 mmol) was quickly added to the stirred pale-yellow solution. The reaction mixture immediately turned black, and after 1 min of stirring, Et_2O (3 mL) was added, and the mixture filtered to remove a black precipitate, presumably graphite. The dark-maroon-purple filtrate was cooled to −35 °C in the freezer for 1 h. The solution was layered with additional Et_2O (15 mL) and stored at −35 °C for 24 h to produce a black/maroon-purple crystalline solid. The mother liquor was decanted, and the solids were rinsed with Et_2O (2 mL) and briefly dried under vacuum to yield **4-Y** as a black/maroon-purple crystalline solid that analyzed as the solvate [K(2.2.2-cryptand)][Cp'_3Y]·THF (252 mg, 51%). Black/maroon-purple single crystals of **4-Y**·THF suitable for X-ray diffraction were grown from THF/Et_2O at −35 °C. The complex retained its THF even under vacuum for several hours as determined by elemental analysis, X-ray diffraction, and ^{1}H NMR spectroscopy. IR: 3079w, 2946m, 2888m, 2824m, 1480w, 1437w, 1361m, 1301w, 1259w, 1237m, 1174m, 1135m, 1105s, 1082m, 1036m, 950m, 934w, 903m, 832s, 751m, 671w, 626m cm^{-1}. Anal. calcd for $C_{42}H_{75}N_2O_6Si_3Y$·C_4H_8O: C, 55.90; H, 8.46; N, 2.83. Found: C, 55.91; H, 8.86; N, 2.85. UV−vis (THF) λ_{max}, nm (ε, M^{-1} cm^{-1}): 278 (5500 shoulder), 405 (3300 shoulder), 520 (4500), 700 (1500 shoulder).

[K(2.2.2-cryptand)][Cp'_3Pr], 4-Pr. As described for **4-Y**, a pale-blue-green solution of Cp'_3Pr, **1-Pr** (300 mg, 0.543 mmol), and 2.2.2-cryptand (204 mg, 0.542 mmol) in THF (2 mL) was combined with KC_8 (96 mg, 0.71 mmol) to produce **4-Pr** as a black/maroon-purple crystalline solid that analyzed as the solvate [K(2.2.2-cryptand)]-[Cp'_3Pr]·THF (401 mg, 71%). Black/maroon-purple single crystals of **4-Pr**·THF suitable for X-ray diffraction were grown from THF/Et_2O at −35 °C. IR: 3072m, 2946s, 2888s, 2823s, 2479w, 1586w, 1480m, 1436s, 1405w, 1361s, 1301s, 1259s, 1236s, 1172s, 1135s, 1107s, 1082s, 1035s, 949s, 902s, 834s, 747m, 736m, 627m cm^{-1}. Anal. calcd for $C_{42}H_{75}N_2O_6Si_3Pr$·C_4H_8O: C, 53.10; H, 8.04; N, 2.69. Found: C, 52.81; H, 8.20; N, 2.57. UV−vis (THF) λ_{max}, nm (ε, M^{-1} cm^{-1}): 275 (6800 shoulder), 518 (4500), 725 (1500 shoulder).

[K(2.2.2-cryptand)][Cp'_3Gd], 4-Gd. As described for **4-Y**, a pale-yellow solution of Cp'_3Gd, **1-Gd** (300 mg, 0.527 mmol), and 2.2.2-cryptand (199 mg, 0.529 mmol) in THF (2 mL) was combined with KC_8 (100 mg, 0.736 mmol) to produce **4-Gd** as a black/maroon-brown crystalline solid that analyzed as the solvate [K(2.2.2-cryptand)]-[Cp'_3Gd]·THF (513 mg, 92%). Black/maroon-brown single crystals of **4-Gd**·THF suitable for X-ray diffraction were grown from THF/Et_2O at −35 °C. IR: 3076m, 2946s, 2889s, 2825s, 1595w, 1480m, 1446m, 1398w, 1361s, 1301m, 1260m, 1236s, 1176s, 1135s, 1105s, 1082s, 1036s, 949s, 903s, 833s, 750s, 68m, 627m cm^{-1}. Anal. calcd for $C_{42}H_{75}N_2O_6Si_3Gd$·C_4H_8O: C, 52.28; H, 7.92; N, 2.65. Found: C, 52.22; H, 8.17; N, 2.69. UV−vis (THF) λ_{max}, nm (ε, M^{-1} cm^{-1}): 282 (5700), 430 (4400), 630 (1400 shoulder).

[K(2.2.2-cryptand)][Cp'_3Tb], 4-Tb. As described for **4-Y**, a light-yellow solution of Cp'_3Tb, **1-Tb** (284 mg, 0.498 mmol), and 2.2.2-cryptand (187 mg, 0.497 mmol) in THF (2 mL) was combined with KC_8 (87 mg, 0.64 mmol) to produce **4-Tb** as a black/maroon-brown crystalline solid that analyzed for the solvate [K(2.2.2-cryptand)]-[Cp'_3Tb]·THF (426 mg, 81%). Black/maroon-brown single crystals of **4-Tb**·THF suitable for X-ray diffraction were grown from THF/Et_2O at −35 °C. IR: 3077w, 2947m, 2888m, 1480w, 1447m, 1361m, 1301m, 1259m, 1236m, 1176m, 1135m, 1105s, 1082m, 1036m, 950m, 903m, 832s, 751s, 673m, 627m cm^{-1}. Anal. calcd for $C_{42}H_{75}N_2O_6Si_3Tb$·C_4H_8O: C, 52.20; H, 7.90; N, 2.65. Found: C, 52.02; H, 8.06; N, 2.55. UV−vis (THF) λ_{max}, nm (ε, M^{-1} cm^{-1}): 280 (6300), 400 (4400 shoulder), 464 (4800), 635 (1500 shoulder).

[K(2.2.2-cryptand)][Cp'_3Ho], 4-Ho. As described for **4-Y**, a yellow solution of Cp'_3Ho, **1-Ho** (236 mg, 0.409 mmol), and 2.2.2-cryptand (154 mg, 0.409 mmol) in THF (2 mL) was combined with KC_8 (56 mg, 0.41 mmol) to produce **4-Ho** as a black/maroon-purple crystalline solid that analyzed as the solvate [K(2.2.2-cryptand)][Cp'_3Ho]·THF (283 mg, 65%). Black/maroon-purple single crystals of **4-Ho**·THF suitable for X-ray diffraction were grown from a concentrated solution in THF/Et_2O at −35 °C. IR: 3080w, 2947m, 2888s, 2820m, 1480w, 1447m, 1361m, 1301m, 1259m, 1236m, 1175m, 1135m, 1105s, 1081m, 1036m, 983w, 950m, 934m, 903m, 832s, 752s, 625m cm^{-1}. Anal. calcd for $C_{42}H_{75}N_2O_6Si_3Ho$·C_4H_8O: C, 51.90; H, 7.86; N, 2.63. Found: C, 51.62; H, 8.11; N, 2.58. UV−vis (THF) λ_{max}, nm (ε, M^{-1} cm^{-1}): 280 (5800 shoulder), 400 (3400 shoulder), 499 (4600), 650 (1500 shoulder).

dx.doi.org/10.1021/ja403753j | J. Am. Chem. Soc. 2013, 135, 9857−9868

[K(2.2.2-cryptand)][Cp′$_3$Er], 4-Er. As described for **4-Y**, a pale-orange solution of Cp′$_3$Er, **1-Er** (350 mg, 0.604 mmol), and 2.2.2-cryptand (228 mg, 0.606 mmol) in THF (2 mL) was combined with KC_8 (82 mg, 0.60 mmol) to produce **4-Er** as a black/maroon-purple crystalline solid that analyzed as the solvate [K(2.2.2-cryptand)][Cp′$_3$Er]·THF (365 mg, 57%). Black/maroon-purple single crystals of **4-Er**·THF suitable for X-ray diffraction were grown from THF/Et_2O at −35 °C. IR: 3081w, 2947m, 2888s, 2825m, 1480w, 1447m, 1361m, 1301m, 1259m, 1236m, 1175m, 1135m, 1105s, 1082m, 1036m, 950m, 934w, 903m, 832s, 768w, 752m, 672w, 630m cm^{-1}. Anal. calcd for $C_{42}H_{75}N_2O_6Si_3Er{\cdot}C_4H_8O$: C, 51.79; H, 7.84; N, 2.63. Found: C, 51.79; H, 7.91; N, 2.61. UV−vis (THF) λ_{max}, nm (ε, M^{-1} cm^{-1}): 276 (6000), 400 (3000), 502 (4000), 650 (1500 shoulder).

[K(2.2.2-cryptand)][Cp′$_3$Lu], 4-Lu. A light yellow solution of Cp′$_3$Lu, **1-Lu** (184 mg, 0.314 mmol), and 2.2.2-cryptand (118 mg, 0.313 mmol) in 2:1 Et_2O/THF (1 mL) was mixed with KC_8 (55 mg, 0.40 mmol) and immediately filtered to remove a black solid, presumably graphite. The dark-maroon-purple filtrate was collected in a cold vial and quickly placed in the freezer at −35 °C for 1 h. Layering with additional cold Et_2O (18 mL, −35 °C) and storing at −35 °C for 24 h produced **4-Lu** as a black/maroon-purple crystalline solid that analyzed for the solvate [K(2.2.2-cryptand)][Cp′$_3$Lu]·THF (138 mg, 41%). Black/maroon-purple single crystals of **4-Lu**·THF suitable for X-ray diffraction were grown from a concentrated solution in THF/Et_2O at −35 °C. IR: 3083w, 2947m, 2888s, 2826m, 1480w, 1437m, 1361m, 1301m, 1259m, 1235s, 1174s, 1135s, 1105s, 1081s, 1036s, 949m, 934m, 903m, 832s, 770m, 752s, 672w, 629m cm^{-1}. Anal. calcd for $C_{42}H_{75}N_2O_6Si_3Lu{\cdot}C_4H_8O$: C, 51.42; H, 7.79; N, 2.61. Found: C, 51.16; H, 7.95; N, 2.57. UV−vis (THF) λ_{max}, nm (ε, M^{-1} cm^{-1}): 275 (6800 shoulder), 518 (4500), 725 (1500 shoulder).

X-ray Data Collection, Structure Determination, and Refinement. Crystallographic details for compounds **1-Pr**, **1-Gd**, **1-Tb**, **2-Tb**, **2-Tb′**, **3-Tb**, **4-Y**, **4-Pr**, **4-Gd**, **4-Tb**, **4-Ho**, **4-Er**, and **4-Lu** are summarized in Tables 2 and 3 and in the Supporting Information.

Table 2. Selected Bond Distances (Å) and Angles (°) for [(18-crown-6)K][Cp′$_3$Tb], 2-Tb, {[(18-crown-6)K][Cp′$_3$Tb]}$_n$, 2-Tb′, and {[(18-crown-6)K]$_2$(μ-Cp′)}{Cp′$_3$Tb}, 3-Tb[a]

	2-Tb	2-Tb′	3-Tb
Tb1−Cnt1	2.444	2.450	2.446
Tb1−Cnt2	2.453	2.462	2.464
Tb1−Cnt3	2.441	2.440	2.452
K1···C(Cp′)[b]	3.060(2), C19	3.035(6), C19	2.968(2), C27
	3.084(2), C18	3.254(7), C18	3.034(2), C26
		3.062(7), C10	
		3.522(7), C11	
K2···C(Cp′)[b]	–	–	2.950(2), C27
			3.029(2), C26
Cnt1−Tb1−Cnt2	118.6	118.8	123.0
Cnt1−Tb1−Cnt3	117.8	118.3	118.7
Cnt2−Tb1−Cnt3	123.2	122.8	118.3

[a]Cnt1, Cnt2, and Cnt3 are the centroids of C1−C5, C9−C13, and C17−C21, respectively. [b]For each Cp′ ring adjacent to K, only the two closest K···C distances are listed.

Computational Details. Density functional theory (DFT) calculations were carried out for **1-Ln** and **4-Ln** for Ln = Pr, Gd, Tb, and Lu. Large 4f-in-core effective core potentials (ECPs) and corresponding quasi-relativistic basis sets[49] were used for Pr, Gd, and Tb, while small-core ECPs[50] and def-TZVP basis sets[51] were used for Lu. The chosen pseudopotentials enforce a fixed 4f^n occupation for the lanthanides (n = 2 for Pr, 7 for Gd, and 8 for Tb). The appropriateness of this configuration was established by small-core calculations treating the 4f shell explicitly (see Supporting Information) as well as prior experience with Ho and Er.[2] Solvation effects were taken into account through the continuum solvation model (COSMO)[52] using the dielectric constant of THF (ε = 7.520).[53] Time-dependent DFT (TDDFT) calculations[54] were also performed to simulate the UV−vis spectrum for **4-Ln**. A full description of the computational methods is reported in the Supporting Information.

Table 3. Experimental and Calculated Average Ln−(Cp′ centroid) Distances (Å) in Cp′$_3$Ln, 1, and [K(2.2.2-cryptand)][Cp′$_3$Ln], 4

	experimental		calculated	
compound	Ln−(Cp′ centroid)$_{avg}$	difference	Ln−(Cp′ centroid)$_{avg}$	difference
1-Pr/4-Pr	2.508/2.535	0.027	2.556/2.590	0.034
1-Gd/4-Gd	2.437/2.468	0.031	2.479/2.502	0.023
1-Tb/4-Tb	2.423/2.454	0.031	2.460/2.493	0.033
1-Y/4-Y	2.405/2.436	0.031	2.416/2.446	0.030
1-Ho/4-Ho	2.394/2.426	0.032	2.437/2.466	0.029
1-Er/4-Er	2.386/2.416	0.030	2.422/2.454	0.032
1-Lu/4-Lu	2.361/2.392	0.031	2.361/2.385	0.024

RESULTS

Tb^{2+}. Despite the calculated −3.7 V vs NHE reduction potential for Tb^{3+} (Table 1), K (−2.9 V vs NHE) reacts with Cp′$_3$Tb, **1-Tb**, in the presence of 18-crown-6 in Et_2O at −35 °C under argon to produce a dark-maroon-brown solution similar to those of Y^{2+}, Ho^{2+}, and Er^{2+} formed via eq 1. The dark-maroon-brown crystals initially isolated from this reaction were analyzed by X-ray diffraction and provided the first crystallographic evidence for the Tb^{2+} ion in a molecular complex, {[K(18-crown-6)]$_2$(μ-Cp′)}{Cp′$_3$Tb}, **3-Tb**, eq 4. The structure of **3**, Figure 1,

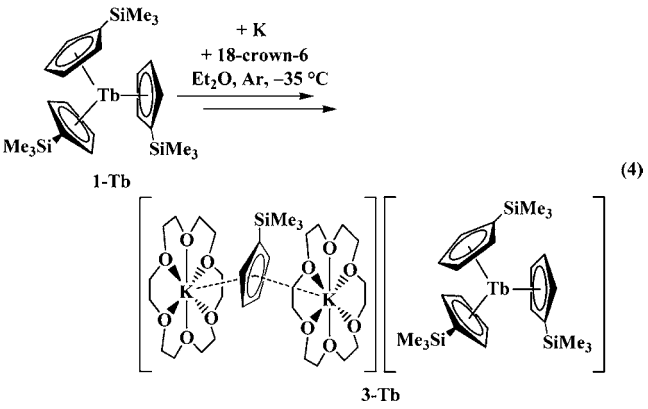

differed from the [(18-crown-6)K][Cp′$_3$Ln], **2**, products in eq 1 in that the cation was not located adjacent to a cyclopentadienyl ring of the anion and the cation was a dipotassium cyclopentadienyl inverse sandwich.[55−57]

The countercation in **3** contained an extra equivalent of K(18-crown-6)Cp′ compared to the products, **2**, of eq 1. Since K(18-crown-6)Cp′ had been observed to be a common decomposition product of **2-Y**, **2-Ho**, and **2-Er**, this was consistent with the terbium analog being thermally unstable as well. Subsequent crystallizations using more concentrated solutions provided crystals of [(18-crown-6)K][Cp′$_3$Tb], **2-Tb**, Figure 2, a compound that is isomorphous with the other analogs of **2** and is likely the precursor to **3-Tb**, Scheme 1. **2-Tb** could be prepared in 30% yield using the method of flash reduction with KC_8 previously reported for **2-Ho** and **2-Er**.[2]

Attempts to generate crystals of **3-Tb** via Scheme 1 by directly adding KCp′ and 18-crown-6 to solutions of **2-Tb** or by performing the initial reduction reaction in the presence of excess KCp′ and 18-crown-6 only resulted in the isolation of **2-Tb** and

dx.doi.org/10.1021/ja403753j | J. Am. Chem. Soc. 2013, 135, 9857−9868

Scheme 1. Three Crystalline Complexes of Tb^{2+}

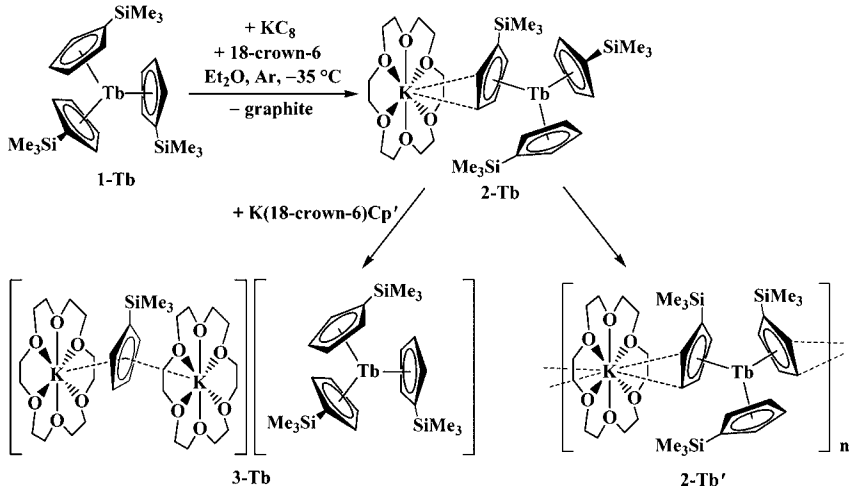

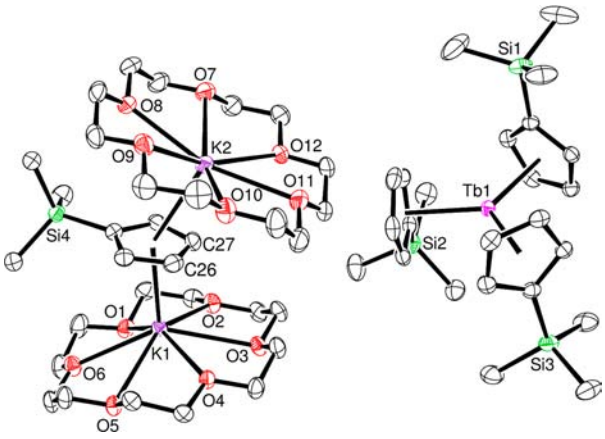

Figure 1. Molecular structure of $\{[(18\text{-crown-6})K]_2(\mu\text{-}Cp')\}\{Cp'_3Tb\}$, **3-Tb**, with thermal ellipsoids drawn at the 50% probability level and hydrogen atoms omitted for clarity.

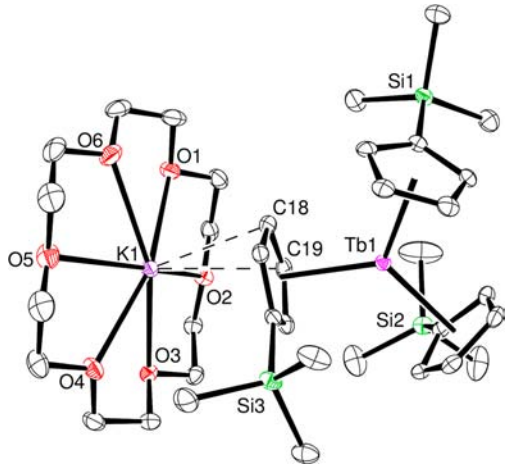

Figure 2. Molecular structure of $[(18\text{-crown-6})K][Cp'_3Tb]$, **2-Tb**, with thermal ellipsoids drawn at the 50% probability level and hydrogen atoms omitted for clarity.

the crystallization of yet another form of a Tb^{2+} complex, $\{[(18\text{-crown-6})K][Cp'_3Tb]\}_n$, **2-Tb′**, a polymeric isomer of **2-Tb** that cocrystallizes with free 18-crown-6. The structure of **2-Tb′**, Figure 3, shows crystallographically equivalent units of $[(18\text{-crown-6})K][Cp'_3Tb]$ monomers connected via K···Cp′ interactions to form a polymeric chain. The location of the potassium atoms between Cp′ rings is not symmetrical, as demonstrated by the difference in bond distances between potassium and the two closest carbon atoms of each ring: 3.035(6) Å (K1−C19) and 3.254(7) Å (K1−C18) vs 3.062(7) Å (K1−C10) and 3.522(7) Å (K1−C11). In comparison, K−C distances are 2.99(1)−3.04(1) Å in KCp'[58] and 3.357−3.399 Å in $[K(18\text{-crown-6})(\text{toluene})_x]^+$ complexes.[59] The two polymorphs of Tb^{2+}, **2-Tb** and **2-Tb′**, were only distinguishable by X-ray crystallography, as both are black/maroon-brown solids that have identical spectral features and similar elemental analyses. Table 2 shows the metrical data for the three Tb^{2+} complexes. Neither the bond distances nor the angles in the $[Cp'_3Tb]^{1-}$ anions of **2-Tb**, **2-Tb′**, and **3-Tb** are significantly affected by the cation or its proximity to a cyclopentadienyl ring bound to terbium.

The fact that potassium reduction of Cp'_3Tb in the presence of 18-crown-6 could lead to three different crystalline forms of Tb^{2+} revealed the flexibility of the $[Cp'_3Ln]^{1-}$ anion in forming isolable crystalline complexes. The isolation of **3-Tb** was particularly significant in several respects. First, it was the first new Ln^{2+} Cp′ complex in which the $[(18\text{-crown-6})K]^{1+}$ countercation was not oriented toward one of the three cyclopentadienyl rings around the Ln^{2+} ion. This demonstrated that the $[Cp'_3Ln]^{1-}$ ion could exist without a proximal alkali metal. Second, the structure of **3-Tb** showed that the $[(18\text{-crown-6})K]^{1+}$ cation was not essential for isolating these ions. Finally, trapping an (18-crown-6)KCp′ moiety in the countercation of **3-Tb** reinforced the suspicion that decomposition of complexes of **2** could involve dissociation of the $(Cp')^{1-}$ ring oriented toward the $[K(18\text{-crown-6})]^{1+}$ cation. Elimination of this K···Cp′ structural feature could lead to greater stability.

2.2.2-Cryptand. To explore these ideas, 2.2.2-cryptand[43,60] was examined as an alternative to 18-crown-6 for stabilizing K^{1+}. Reactions were initially attempted with Y, Ho, Er, and Tb. As shown in eq 5, this generated a new series of Ln^{2+} complexes, $[K(2.2.2\text{-cryptand})][Cp'_3Ln]$, **4**, Figure 4, in which the potassium was not oriented toward the $[Cp'_3Ln]^{1-}$ anion. These cryptand complexes proved to be significantly more stable than the 18-crown-6 compounds, **2**, such that eq 5 did not require −35 °C in Et_2O as necessary for eq 1, but could be conducted at room temperature and in THF if the reaction time was short (<5 min).

dx.doi.org/10.1021/ja403753j | J. Am. Chem. Soc. 2013, 135, 9857−9868

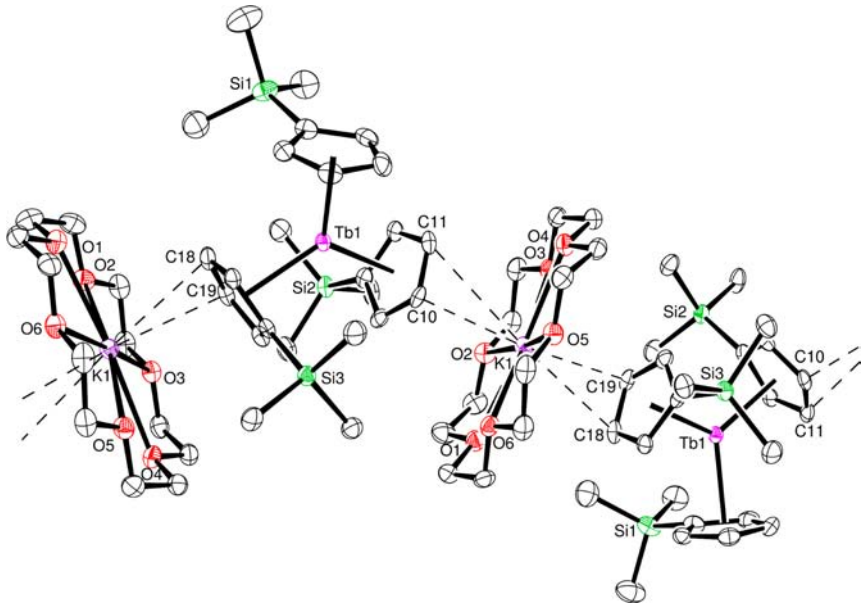

Figure 3. Two repeat units in the structure of $\{[(18\text{-crown-6})K][Cp'_3Tb]\}_n$, **2-Tb′**, with thermal ellipsoids drawn at the 50% probability level and hydrogen atoms omitted for clarity.

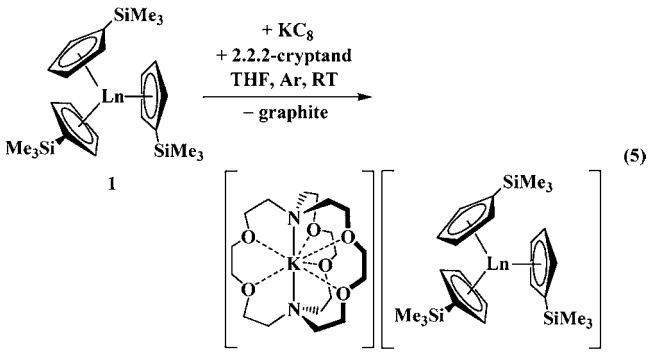

Gd^{2+} and Pr^{2+}. Since the stability of the Ln^{2+} complexes was improved with 2.2.2-cryptand, the reaction shown in eq 5 was applied to the lanthanide theoretically most difficult to reduce,[5] the half-filled shell $4f^7$ Gd^{3+}. The method was also examined with praseodymium, a metal with the potential to be problematic since it is much larger than Tb, Ho, Er, and Y; a praseodymium product analogous to **4** might be more reactive due to coordinative unsaturation. As shown in eq 5, this approach provided the first examples of molecular Pr^{2+} and Gd^{2+} complexes, **4-Pr** and **4-Gd**, whose crystal structures proved to be isomorphous with **4-Y**, **4-Tb**, **4-Ho**, and **4-Er**, Figure 4.

Lu^{2+}. Previously, we reported that deep-blue solutions generated at low temperatures from the reaction of $[(Me_3Si)_2N]_3Lu$ with K and 18-crown-6 could reduce CO, a result that provided chemical evidence for the existence of Lu^{2+} in solution.[61] However, neither spectroscopic nor crystallographic evidence for Lu^{2+} could be obtained in that system. Once a reliable preparation for analytically pure Cp'_3Lu was developed,[46] the method of reduction shown in eq 5 was applied to lutetium as well. Although this reaction formed dark-maroon-purple colored solutions like the other examples in eq 5, crystallization proved more difficult with this smallest lanthanide apparently due to lower stability at room temperature (see below). Ultimately, crystals were obtained from more concentrated reaction mixtures that were immediately filtered, layered with cold Et_2O, and cooled to −35 °C. This provided the first crystallographic evidence for a molecular Lu^{2+} complex,

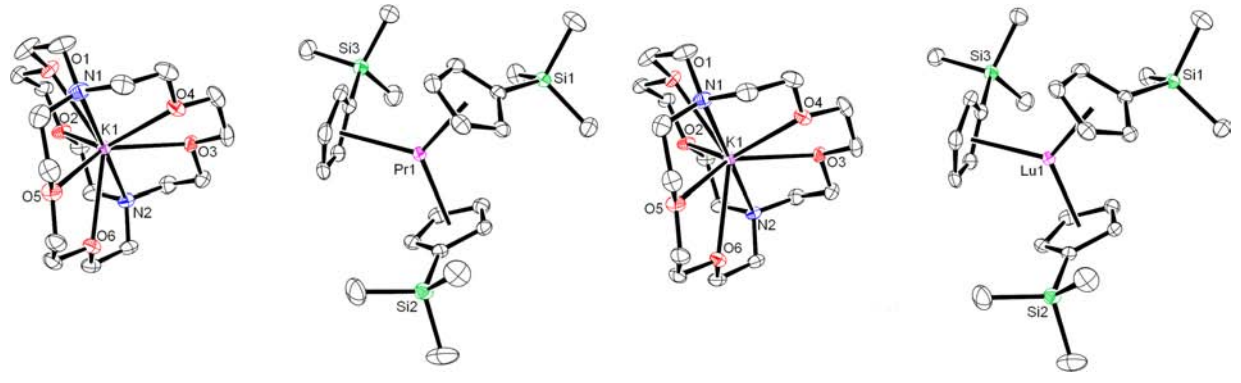

Figure 4. Molecular structures of $[K(2.2.2\text{-cryptand})][Cp'_3Ln]$, **4**, (Ln = Y, Pr, Gd, Tb, Ho, Er, Lu) with thermal ellipsoids drawn at the 50% probability level and hydrogen atoms omitted for clarity. These complexes are all isomorphous, so only the structures of the analogs with the largest metal, Pr, and the smallest metal, Lu, are shown.

dx.doi.org/10.1021/ja403753j | J. Am. Chem. Soc. 2013, 135, 9857−9868

[K(2.2.2-cryptand)][Cp′$_3$Lu], **4-Lu**, a complex isomorphous with the others, Figure 4. Hence, crystalline molecular complexes containing Ln^{2+} ions are now known for all the lanthanides in the series except for radioactive promethium.

Theoretical Analysis. DFT calculations were performed to predict the properties of these new divalent ions. Calculations on $[Cp'_3Pr]^{1-}$, $[Cp'_3Gd]^{1-}$, $[Cp'_3Tb]^{1-}$, and $[Cp'_3Lu]^{1-}$ gave similar results, and the HOMO and LUMO for the gadolinium complex are shown in Figure 5. In each case, the calculations

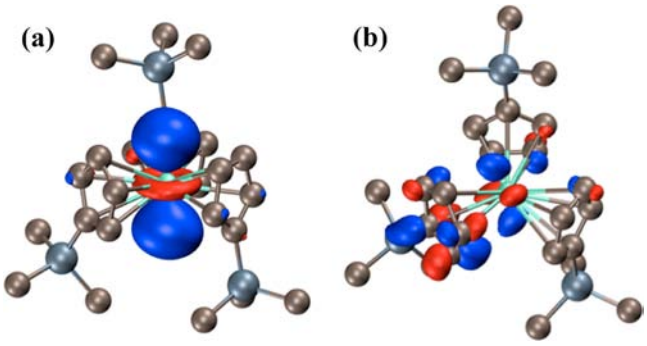

Figure 5. Molecular orbital plots of the anion in **4-Gd**: (a) the 119a orbital (HOMO) and (b) the 121a orbital (LUMO+1), using a contour value of 0.06. The predicted excitation wavelength from the HOMO to LUMO+1 is 744 nm (see the Supporting Information for details).

show that the HOMO of the Ln^{2+} complexes has mainly $5d^1$ character, i.e., these ions are best described as $4f^n5d^1$ species. This $4f^{14}5d^1$ configuration is necessary for Lu^{2+} since Lu^{3+} already has a filled 4f shell. The $4f^75d^1$ configuration for Gd^{2+} allows the half-filled 4f shell to be preserved. More general reasons also exist to rationalize why these ions, as well as Pr^{2+} and Tb^{2+}, prefer to adopt $4f^n5d^1$ configurations rather than $4f^{n+1}$ configurations: (i) the lanthanide 4f orbitals have a limited radial extension in comparison to the 5d orbitals that diminishes the possibility for a stabilizing interaction with the orbitals of the Cp′ ligands;[62] and (ii) for the gas phase ions, the splitting between the 5d and 4f shells for Pr, Tb, Ho, and Er is known to decrease with the decrease in metal oxidation state[22] such that splitting induced by a ligand field could place one or more 5d orbitals lower in energy than the 4f orbitals. Calculations on solid-state halides, chalcogenides, and pnictides of Ln^{2+} compounds also show that the 4f and 5d orbitals are similar in energy in the +2 oxidation state.[44]

Consistent with this, the measured and predicted physical properties for **4-Pr** and **4-Tb** show great similarity to those for the $[Cp'_3Ho]^{1-}$, $[Cp'_3Er]^{1-}$, and $[Cp'_3Y]^{1-}$ ions, which were previously determined to be $4f^n5d^1$ and $4d^1$ species.[1,2] Due to the compact nature of the 4f orbitals, near-degeneracies may arise between two or more configurations with different f-occupation,[63−65] which calls into question the use of single-reference methodologies. Nevertheless, the properties predicted by DFT using the chosen f-in-core ECPs are indeed consistent with the physical properties of these new complexes (see below).

Structural Data. Crystallographic information was also obtained for the trivalent Cp′$_3$Ln complexes **1-Pr**, **1-Gd**, and **1-Tb** (Figure S1, Table S1). Comparisons of Ln−(Cp′ centroid) bond distances in the seven examples of **4** with those in the Ln^{3+} precursors, **1**, Table 3, show that in each case the distances in the Ln^{2+} complexes are ∼0.03 Å longer. This is similar to the situation observed for the Ln^{2+} ions in **2** (Ln = Y,[1] Ho,[2] Er,[2] Tb) and for [K(18-crown-6)(OEt$_2$)][Cp″$_3$La] and [K(2.2.2-cryptand)][Cp″$_3$La].[43] The computed structural data using TZVP basis sets also show a lengthening of the average Ln−(Cp′ centroid) distance upon reduction by 0.023−0.034 Å for the entire series (see Supporting Information). In contrast, for Eu^{2+}, Yb^{2+}, Sm^{2+}, Tm^{2+}, Dy^{2+}, and Nd^{2+}, addition of an electron to a $4f^n$ Ln^{3+} ion complex has historically made a $4f^{n+1}$ Ln^{2+} ion complex that has metal ligand distances 0.05−0.2 Å longer than those of the Ln^{3+} analog.[3,18,66−69] The small changes in bond distance with oxidation state in **2** and **4** are more characteristic of transition-metal chemistry[70] and fit with the assignment of $4f^n5d^1$ rather than $4f^{n+1}$ configurations for these ions.

UV−vis Spectroscopy. The UV−vis spectra of the new Pr^{2+}, Gd^{2+}, Tb^{2+}, and Lu^{2+} complexes are also suggestive of a $4f^n5d^1$ configuration. The spectra of the six lanthanide examples of **4** are similar and match that of $4d^1$ Y^{2+}, Figure 6. Hence, these spectra are reasonable for nd^1 complexes in a trigonal field. As in the case of the $[Cp'_3Y]^{1-}$ ion,[2] TDDFT predicts for each example of **4**

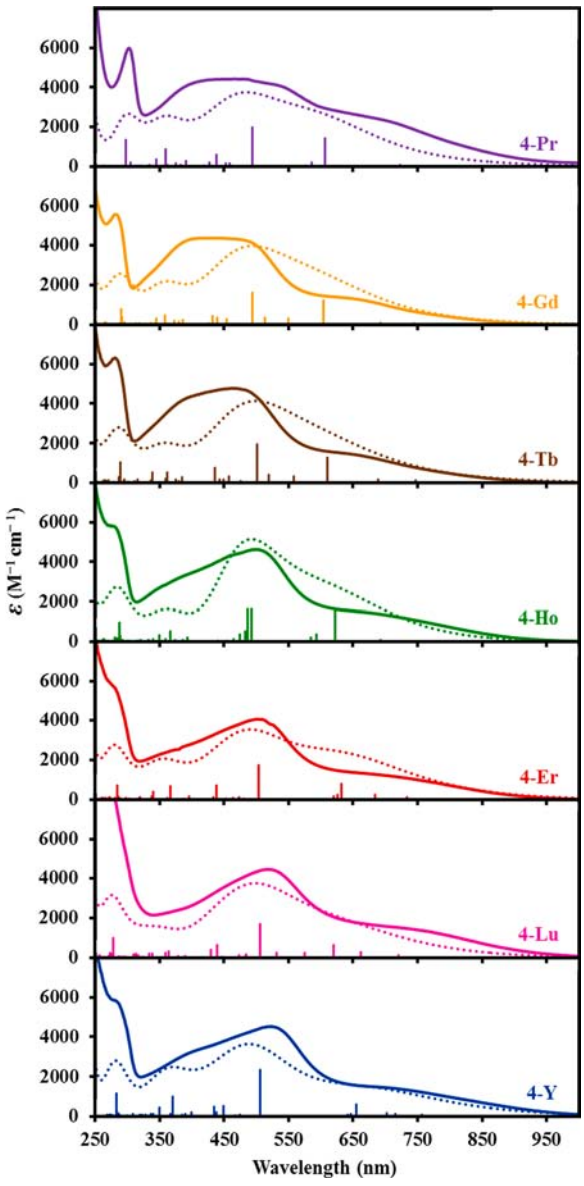

Figure 6. Experimental (solid) and calculated (dotted) UV−vis spectra of [K(2.2.2-cryptand)][Cp′$_3$Ln], **4**, (Ln = Pr, Gd, Tb, Ho, Er, Lu, Y) in THF at 298 K, with pertinent theoretical excitations shown as vertical lines and theoretical extinction coefficients scaled down by a factor of 4.

dx.doi.org/10.1021/ja403753j | J. Am. Chem. Soc. 2013, 135, 9857−9868

several excitations with appreciable oscillator strength between 300 and 800 nm, which make up the two main bands in the spectrum for each complex. A summary of the characteristic excitations from each band is given in Table S19. In the low-energy region (λ > 600 nm), the predicted excitations are a mixture of d→d and d→π* in which the d→d transitions have significant ligand character. The transitions in the higher energy band (300−600 nm) become increasingly metal-to-ligand d→π* charge transfer with the decrease in wavelength. The low-energy transitions seem to originate from the $4f^n5d^1$ occupation since excitations computed using a $4f^{n+1}$ ECP lack any prominent peaks in the long wavelength region, as was shown previously[2] for Ho^{2+}. This analysis is consistent with previous calculations on $(\eta^5\text{-}C_5H_5)_3M$ complexes of lanthanides and actinides where the three $(C_5H_5)^{1-}$ rings provide a pseudo-D_{3h} coordination environment.[71−73]

Thermal Stability. The decomposition of the seven examples of **4** in THF at 298 K was monitored by following the disappearance of the most intense absorbance at λ_{max} in the visible region at 15 min intervals. For each metal except Lu, the plot of 1/[**4**] vs time is linear and consistent with a rate-determining step that is second-order in **4**, Figure 7. Complex **4-Lu**, however, was found to be much less stable: it showed 99% decomposition within 2 h. In addition, the initial reaction seems to follow first-order kinetics with respect to **4-Lu**, as the plot of ln[**4**] vs time is linear, Figure S4a. Although the mechanism of these decomposition reactions is unclear at this time, the data do provide a preliminary stability order of Pr^{2+} > Gd^{2+} > Tb^{2+} > Ho^{2+} > Er^{2+} > Y^{2+} > Lu^{2+}, with initial half-lives of 20 days, 3.7 days, 22 h, 3.5 h, 2.5 h, 2.3 h, and 19 min, respectively, at 3 mM concentrations. In comparison, the 18-crown-6 analogs, **2**, in Et_2O at 298 K have half-lives of 6.1 min to 1.5 h, Figure S4b. The order of stability does not match the order of reduction potentials in Table 1, but since those were calculated for $4f^n \rightarrow 4f^{n+1}$ reductions not $4f^n \rightarrow 4f^n5d^1$ (except for Y^{2+} and Lu^{2+}, which must necessarily be nd^1 ions), they cannot be expected to reflect the stability of the new ions. The order of decomposition does seem to follow a periodic trend that could be related to radial size.

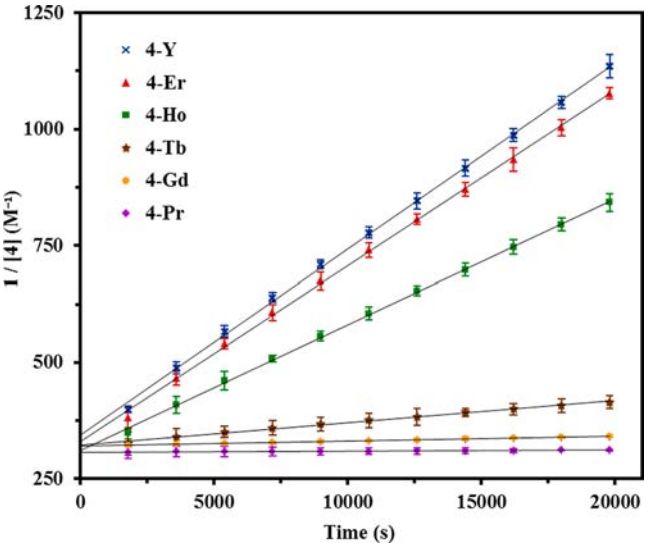

Figure 7. Kinetic data for the decomposition of ~3 mM solutions of [K(2.2.2-cryptand)][Cp′$_3$Ln], **4**, (Ln = Y, Er, Ho, Tb, Gd, Pr) in THF under argon at 298 K.

EPR Spectroscopy. The only well-resolved X-band EPR spectra observed so far for the products of eq 5 are the spectra of **4-Y**, **4-Lu**, and **4-Gd** obtained as THF solutions at 295 and 77 K, Figure 8. These are the ions with empty, filled, and half-filled 4f shells, respectively. The lack of definitive EPR signals for the other ions at these temperatures is not unexpected since (i) the anisotropy of the other paramagnetic lanthanide ions often allows EPR data to be obtained only on oriented single crystals of the ions doped into diamagnetic matrices[74] and (ii) rapid spin−lattice relaxation of the electronic excited states of these metals usually prevents their EPR spectra from being observed above 20 K.[74−76]

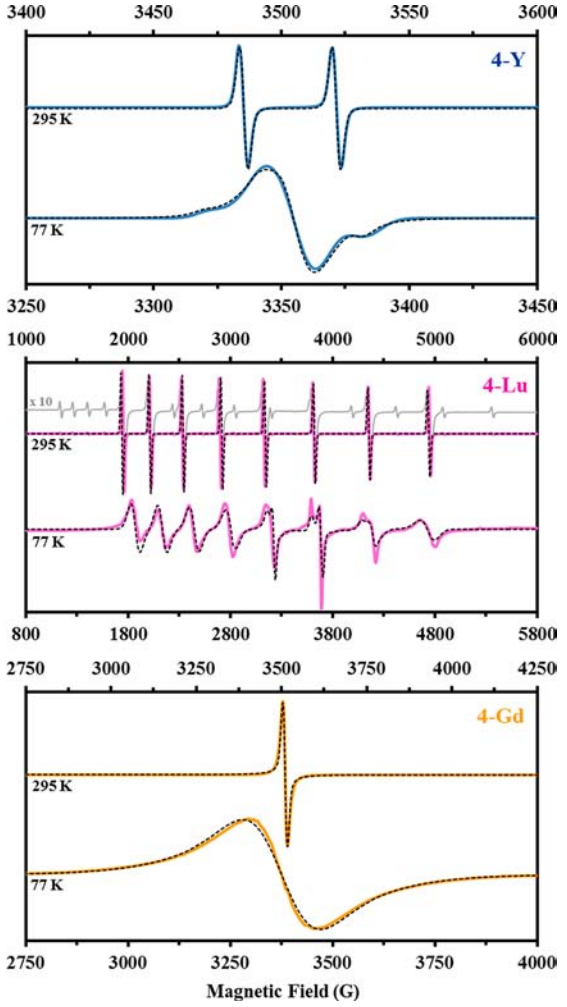

Figure 8. Experimental (solid) and simulated (dashed) X-band EPR spectra of 10 mM solutions of **4-Y**, **4-Lu**, and **4-Gd** in THF at 295 and 77 K.

The room temperature spectra of **4-Y**, **4-Lu**, and **4-Gd** each display isotropic signals with g_{iso} = 1.991, 1.974, and 1.987, respectively (Figure 8, Table 4), which are consistent with metal-based $S = {}^1/_2$ spin systems. The **4-Y** spectrum contains a doublet as expected for an unpaired electron interacting strongly with the $I = {}^1/_2$ nucleus of ^{89}Y (100% natural abundance). The A_{iso} = 36.6 G hyperfine coupling constant (Table 4) is identical to that previously observed for **2-Y**.[1]

The eight line pattern observed for **4-Lu** is reasonable for a $4f^{14}5d^1$ ion since ^{175}Lu is an $I = {}^7/_2$ nucleus (97.4% natural abundance). The average ^{175}Lu hyperfine coupling constant, A_{iso}

dx.doi.org/10.1021/ja403753j | J. Am. Chem. Soc. 2013, 135, 9857−9868

Table 4. EPR Spectroscopic Parameters of 4-Y, 4-Lu, and 4-Gd

		g value	*A* (Hz)	*A* (G)
4-Y	RT	g_{iso} = 1.991	^{89}Y A_{iso} = 102	^{89}Y A_{iso} = 36.6
	77 K	$g_{\|}$ = 2.006; $g_{\perp}$ = 1.982	^{89}Y $A_{\|}$ = 50; $A_{\perp}$ = 55	^{89}Y $A_{\|}$ = 18; $A_{\perp}$ = 20
4-Lu	RT	g_{iso} = 1.974	^{175}Lu A_{iso} = 1184 ^{176}Lu A_{iso} = 833	^{175}Lu A_{iso} = 428.5 ^{176}Lu A_{iso} = 302
	77 K	$g_{\|}$ = 1.998; $g_{\perp}$ = 1.966	^{175}Lu $A_{\|}$ = 1080; $A_{\perp}$ = 1145	^{175}Lu $A_{\|}$ = 386.2; $A_{\perp}$ = 416.1
4-Gd	RT	g_{iso} = 1.987	–	–
	77 K	g_{iso} = 1.984	–	–

= 428.5 G, is the largest observed to date for any lutetium complex. In comparison, the Lu^0 bis(arene) complex, Lu-(η^6-^{t}Bu$_3$C$_6$H$_3$)$_2$, that formally contains a lutetium-based radical (atomic ground-state configuration of $4f^{14}5d^16s^2$), displayed a weak octet EPR signal with hyperfine coupling of 95 G.[77] In contrast, the metallofullerene Lu@C_{82}, which was determined to contain a Lu^{3+} ion inside a fullerene radical trianion, showed a barely resolvable coupling to ^{175}Lu of only 1.25 G in the EPR spectrum.[78]

The significantly larger coupling constant in **4-Lu** is on the same order of magnitude as the Zeeman splitting energy, which gives rise to unequal peak-to-peak distances across the spectrum due to a relatively nonlinear separation of spin states with increasing magnetic field.[79,80] The variable line width of the eight resonances, more pronounced in the 77 K spectrum, is also indicative of a metal-centered radical whose spin relaxation is heavily dependent on the spin angular momentum of the lutetium nucleus.[80] Upon magnification of the room temperature spectrum of **4-Lu**, a second set of peaks can be resolved: a 15 line pattern arising from hyperfine coupling to the $I = 7$ ^{176}Lu nucleus (2.59% natural abundance).

As shown in Figure 8, a sharp signal is observed for **4-Gd** at room temperature that could be attributed to a $4f^75d^1$ configuration with the $4f^7$ component making no observable contribution. In comparison, the $4f^7$ Gd^{3+} precursor, **1-Gd**, shows no signal under similar conditions and only a very broad, shallow signal at much higher concentrations and magnified power. If the electron configuration of the Gd^{2+} ion were $4f^8$ (isoelectronic to Tb^{3+}), the resulting magnetic anisotropy and integer spin state of $S = 4$ would be expected to prevent any EPR signal from being observed in perpendicular mode at room temperature. Interestingly, no hyperfine coupling is observed in the gadolinium spectrum despite the presence of two $I = {}^3/_2$ isotopes, ^{155}Gd and ^{157}Gd (14.8% and 15.7% natural abundance, respectively). It is possible that the paramagnetic environment of the $4f^7$ electrons in the Gd^{2+} ion renders this hyperfine interaction unresolved.

At 77 K, the signals for all three complexes display a significant amount of line broadening. While the low-temperature EPR spectrum of **4-Gd** remains isotropic, the spectra of **4-Y** and **4-Lu** exhibit axial signals, as modeled by spectral simulation, and are consistent with, but not definitive for, a trigonal crystal field around the Ln^{2+} ions. The low-temperature spectrum of **4-Y** was best modeled as an overlapping doublet axial signal; simulations for $g_x \neq g_y \neq g_z$ were unsuccessful.

DISCUSSION

The potassium-based reduction of the Er^{3+} complex, Cp′$_3$Er, to make the Er^{2+} complex, [(18-crown-6)K][Cp′$_3$Er], **2-Er**, eq 1,[2] suggested that the calculated redox potentials of Table 1, e.g., the −3.1 V for Er^{3+}/Er^{2+}, could not be compared directly with the −2.9 V value generally cited for K^{1+}/K^0. Certainly, both redox potentials are generic values that could have a margin of error that would allow the potassium reduction to occur in specific cases. However, since the Tb^{3+}/Tb^{2+} couple is −3.7 V[5] and potassium-based reduction of Cp′$_3$Tb is observed to make the Tb^{2+} complexes, [(18-crown-6)K][Cp′$_3$Tb], **2-Tb**, {[(18-crown-6)K][Cp′$_3$Tb]}$_n$, **2-Tb′**, and {[K(18-crown-6)]$_2$(μ-Cp′)}{Cp′$_3$Tb}, **3-Tb**, eq 4 and Scheme 1, it became clear that the Table 1 redox potentials could not be taken literally for the Ln^{2+} ions in these organometallic complexes. Since the Table 1 potentials were calculated for $4f^n/4f^{n+1}$ reductions and, as discussed below, the new ions appear to have $4f^n5d^1$ configurations, there is a rationale for this discrepancy.

The Tb^{2+} syntheses were critically informative in another way. The isolation of **3-Tb** with the inverse cyclopentadienyl sandwich cation, {[K(18-crown-6)]$_2$(μ-Cp′)}$^{1+}$, demonstrated that a [K(18-crown-6)]$^{1+}$ cation was not essential to stabilize [Cp′$_3$Ln]$^{1-}$ anions as had been observed for the Y^{2+}, Ho^{2+}, and Er^{2+} complexes.[1,2] Previously, it had seemed possible that potassium interaction with one of the cyclopentadienyl rings would aid in reducing the electron density on the rare earth metal and could be essential to allow the highly reduced Ln^{2+} ion to be isolated. This clearly was not the case in **3** and led to exploration of 2.2.2-cryptand to stabilize the K^{1+} ion.[43] The 2.2.2-cryptand complexes [K(2.2.2-cryptand)][Cp′$_3$Ln], **4**, of Y, Ho, Er, and Tb, all proved to be more thermally stable than the [(18-crown-6)K][Cp′$_3$Ln], **2**, series. In addition, syntheses of **4** could be accomplished at room temperature in THF (albeit with short reaction times) instead of the −35 °C in Et$_2$O conditions for **2**. The greater stability of the cryptand complexes, **4**, is also consistent with the idea that [K(18-crown-6)]$^{1+}$ countercation could provide a pathway for decomposition to form K(18-crown-6)Cp′, which is commonly observed in decomposed samples of **2**.

Utilization of the more favorable 2.2.2-cryptand chelate for potassium allowed the first soluble crystalline molecular complexes of Gd^{2+}, Pr^{2+}, and Lu^{2+} to be isolated as shown in eq 5. Isolation of these ions indicates that Ln^{2+} ions are accessible in solution not only for the traditional +2 ions, Eu^{2+}, Yb^{2+}, Sm^{2+}, Tm^{2+}, Dy^{2+}, and Nd^{2+}, and the metals at the beginning of the series, $La^{2+}$and Ce^{2+}, but also for all the lanthanide metals. The data suggest that radioactive promethium would also have an accessible Ln^{2+} ion since Pm is not unusual in either radial size, calculated redox potential (Table 1), or position in the series.

Preliminary data on the new Ln^{2+} ions suggest that they have electron configurations best described at the single electron approximation level as $4f^n5d^1$, not the $4f^{n+1}$ configurations of the traditional Eu^{2+}, Yb^{2+}, Sm^{2+}, Tm^{2+}, Dy^{2+}, and Nd^{2+} ions. The Ln−C bond distances for both the **2** and **4** series of Ln^{2+}

dx.doi.org/10.1021/ja403753j | J. Am. Chem. Soc. 2013, 135, 9857−9868

complexes as well as in the $[Cp''_3Ln]^{1-}$ complexes of Lappert[43] are all just slightly longer than those of the Ln^{3+} analogs, Cp'_3Ln and Cp''_3Ln. This matches the small changes in radial size commonly seen between different oxidation states in transition-metal complexes[70] and contrasts sharply with the 0.05−0.2 Å differences typically seen between $4f^n$ Ln^{3+} and $4f^{n+1}$ Ln^{2+} complexes. For example, the average Sm−(C_5Me_5 centroid) and Sm−O distances in $(C_5Me_5)_2Sm(THF)_2$ (2.599 and 2.633 Å)[81] are 0.176 and 0.173 Å longer, respectively, than those in $[(C_5Me_5)_2Sm(THF)_2][BPh_4]$ (2.423 and 2.457 Å).[82]

Another indication of the $4f^n5d^1$ configuration of the new Ln^{2+} ions comes from the UV−vis spectroscopic data, Figure 6. The spectra of Pr^{2+}, Gd^{2+}, Tb^{2+}, Ho^{2+}, and Er^{2+} are all very similar to those of $4d^1$ Y^{2+} and $4f^{14}5d^1$ Lu^{2+}. These data are consistent with a d^1 ion in a trigonal planar environment in which electronic transitions from a HOMO a_1' (d_{z^2}) orbital to higher-lying e″ (d_{xz}/d_{yz}, π^*) and e′ ($d_{xy}/d_{x^2-y^2}$, π^*) orbitals in D_{3h} symmetry would be expected.

DFT also supports assignment of the $4f^n5d^1$ configuration to the new Ln^{2+} ions based on the large-core calculations discussed above and on additional calculations detailed in the Supporting Information that explicitly include the 4f shell in the valence. The qualitative agreement between the predicted and experimental UV−vis spectra using the $4f^n$ electron core potentials supports the suspected $5d^1$ occupation, as there are predicted characteristic d→d transitions that match the experimental absorption bands that do not arise for a $4f^{n+1}$ occupation. The large extinction coefficients also indicate the large degree of overlap between unoccupied metal d and ligand π^* orbitals. Since the metal atoms are in a relatively low-oxidation state, the 5d orbitals are lowered to the appropriate energy range for chemical interactions, while the 4f orbitals remain core-like and do not interact strongly with the ligand field. The change in average metal−centroid distance upon reduction is also reproduced to within 0.015 Å of the experimental results at the TZVP level for the entire series.

The EPR data on $4d^1$ Y^{2+}, $4f^{14}5d^1$ Lu^{2+}, and $4f^75d^1$ Gd^{2+} also support these electronic assignments for the new ions. Such spectroscopic data on open shell $4f^n$ configuration ions are typically difficult to obtain due to anisotropy and generally require doped single crystals. However, spectra were observable for these three ions, which have empty, filled, and half-filled 4f shells, respectively. The spectra were indicative of an unpaired electron in a metal-based orbital that, in the case of yttrium and lutetium, exhibited the hyperfine coupling expected for the metal nuclear spins present. If the unpaired electrons were ligand based in these complexes, a narrow signal closer to the *g* value of a free electron showing hyperfine coupling to ^1H and ^{29}Si would be expected.

Although the use of 2.2.2-cryptand provided a series of Ln^{2+} species, **4**, that are more stable than the series containing 18-crown-6 around the potassium, **2** and **3**, the complexes **4** are still highly reactive species. For example, **4-Lu** has a half-life of only 19 min in THF at room temperature under argon. Preliminary data on the decomposition of these ions show the following order of stability: $Pr^{2+} > Gd^{2+} > Tb^{2+} > Ho^{2+} > Er^{2+} > Y^{2+} > Lu^{2+}$. This does not match the order of the calculated redox potentials of Table 1, although this is not surprising since those calculations are based on $4f^{n+1}$ configurations for the open f shell Ln^{2+} ions, not $4f^n5d^1$. The position of Gd^{2+} as the second-most stable of these reactive species could be attributed to the half-filled shell that would be present in a $4f^75d^1$ electron configuration. However, this rationale does not extend to the Lu^{2+} $4f^{14}5d^1$ filled 4f shell ion. Traditionally in the lanthanides, both half-filled and filled shells give enhanced stability as observed for $4f^7$ Eu^{2+} and $4f^{14}$ Yb^{2+}.[5]

The rate at which the Lu^{2+} ion decomposes could be greatly accelerated in this system by the fact that the $(Cp'_3)^{3-}$ ligand environment already approaches a steric extreme for the small Lu^{3+} ion. Indeed, the synthesis of Cp'_3Lu, **1-Lu**, proved to be more challenging than that for the larger metals.[46] If the rate-determining step of the decomposition of these compounds involves loss of a $(Cp')^{1-}$ ligand, then the sterically crowded **4-Lu** would be expected to be less stable than analogs of larger metals. Overall, the stability trend for the different analogs of **4** seems to follow the order of radial size, as is often the case in homologous series of lanthanide complexes. This radial size dependence can be rationalized by decomposition pathways involving loss of a $(Cp')^{1-}$ ligand.

As previously pointed out for the bis(η^6-arene) complexes of zerovalent rare earths, $Ln(\eta^6\text{-}^tBu_3C_6H_3)_2$,[77,83,84] the stability of these reduced metal ion complexes is likely dependent on both steric and electronic factors. That study made correlations with the $4f^{n+1}6s^2 \rightarrow 4f^n5d^16s^2$ promotional energies for free lanthanide atoms,[85] and it is appropriate to compare the stability order above for the Ln^{2+} ions with those energies as well as with the $4f^{n+1} \rightarrow 4f^n5d^1$ promotional energies for free Ln^{2+} ions.[86] These data give some information on the accessibility of the 5d orbital. The data for the atoms and ions are parallel as shown in Figure 9

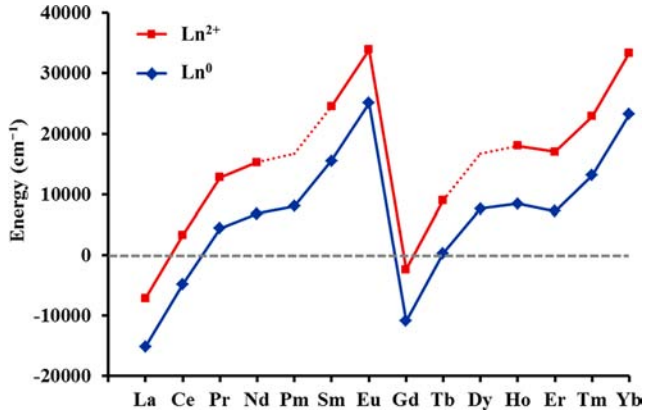

Figure 9. Promotional energies of $4f^{n+1}6s^2 \rightarrow 4f^n5d^16s^2$ transitions in free Ln^0 atoms[85] (blue diamonds) and $4f^{n+1} \rightarrow 4f^n5d^1$ transitions in free Ln^{2+} ions[86] (red squares), with estimated values for Pm^{2+} and Dy^{2+}.

(and in Table S17). For La, Ce, and Gd atoms, these energies are negative. This means that for these elements, the $5d^16s^2$, $4f^15d^16s^2$, and $4f^75d^16s^2$ configurations for the metals are more stable than the $4f^16s^2$, $4f^26s^2$, and $4f^86s^2$ configurations, respectively. In the +2 ion series, the values for La and Gd are negative. This is consistent with previously reported optical excitation spectra of Ln^{2+} ions generated in situ via γ radiation in CaF_2 host crystals, where the ground-state configurations of La^{2+} and Gd^{2+} were concluded to be $5d^1$ and $4f^75d^1$, respectively, and Ce^{2+} and Tb^{2+} were borderline between $4f^{n+1}$ and $4f^n5d^1$.[26] The prior existence of La^{2+} and Ce^{2+} molecular complexes[42,43] and the fact that the Gd^{2+} complex, **4-Gd**, seems to be one of the most stable in the series of **4** match the order of the promotional energies for both atoms and ions in Figure 6. The Gd < Tb < Pr < Er < Ho order of promotional energies does not quite match the order of stability above, $Pr^{2+} > Gd^{2+} > Tb^{2+} > Ho^{2+} > Er^{2+}$, but there are some parallels that should be considered as the detailed

dx.doi.org/10.1021/ja403753j | J. Am. Chem. Soc. 2013, 135, 9857−9868

nature of these new ions becomes further defined. It is likely that several variables affect the relative accessibility and stability of the +2 oxidation state of these metals, including steric factors as mentioned previously.

CONCLUSION

In summary, the +2 oxidation state is accessible to all of the lanthanides in soluble crystalline molecular species. The radioactivity of Pm prevents its examination, but it is reasonable to expect that Pm^{2+} would be accessible like all the other members of the series. The prior expectation that the Tb^{2+}, Pr^{2+}, Gd^{2+}, and Lu^{2+} ions would not be stable as molecular species in solution was largely predicated on the assumption that they would adopt $4f^{n+1}$ electron configurations like the traditional Ln^{2+} ions, Eu^{2+}, Yb^{2+}, Sm^{2+}, Tm^{2+}, Dy^{2+}, and Nd^{2+}. If the $4f^n5d^1$ configuration implied by the preliminary data reported here proves to be the best description of the new ions, this provides an explanation for their existence. The fact that the cryptand-stabilized complexes, **4**, can be synthesized at room temperature vs the −35 °C temperatures needed for the 18-crown-6 complexes, **2**, will significantly aid in exploring the chemistry of these new species. Although the cryptand complexes still decompose in solution, their enhanced thermal stability will facilitate the acquisition of more definitive data on the reactivity and physical properties of these new Ln^{2+} ions.

ASSOCIATED CONTENT

Supporting Information

Additional computational details, spectroscopic information, crystallographic data collection, structure solution, and refinement (PDF), X-ray diffraction details of compounds **1-Pr, 1-Gd, 1-Tb, 2-Tb, 2-Tb′, 3-Tb, 4-Y, 4-Pr, 4-Gd, 4-Tb, 4-Ho, 4-Er**, and **4-Lu** (CIF, CCDC nos. 933988−934000), and DFT-optimized structural coordinates for **1-Pr, 1-Gd, 1-Tb, 1-Lu**, and the anions in **4-Pr, 4-Gd, 4-Tb**, and **4-Lu**. This material is available free of charge via the Internet at http://pubs.acs.org.

AUTHOR INFORMATION

Corresponding Author

wevans@uci.edu; filipp.furche@uci.edu

Notes

The authors declare no competing financial interest.

ACKNOWLEDGMENTS

This paper is dedicated to two pioneers in the field, Professors Michael F. Lappert and Glen B. Deacon. We thank the U.S. National Science Foundation for support of this research under CHE-1010002 (W.J.E.) and CHE-1213382 (F.F.), Professor A. S. Borovik for assistance with EPR and UV−Vis spectroscopy, and Megan E. Fieser for help with the manuscript.

REFERENCES

(1) MacDonald, M. R.; Ziller, J. W.; Evans, W. J. *J. Am. Chem. Soc.* **2011**, *133*, 15914.
(2) MacDonald, M. R.; Bates, J. E.; Fieser, M. E.; Ziller, J. W.; Furche, F.; Evans, W. J. *J. Am. Chem. Soc.* **2012**, *134*, 8420.
(3) Bochkarev, M. N. *Coord. Chem. Rev.* **2004**, *248*, 835 and references therein.
(4) Nief, F. *Dalton Trans.* **2010**, *39*, 6589 and references therein.
(5) Morss, L. R. *Chem. Rev.* **1976**, *76*, 827.
(6) Meyer, G. *Chem. Rev.* **1988**, *88*, 93.
(7) Meyer, G.; Meyer, H.-J. *Chem. Mater.* **1992**, *4*, 1157.
(8) Meyer, G.; Wickleder, M. S. In *Handbook on the Physics and Chemistry of Rare Earths*; Gschneidner, K. A., Jr., Eyring, L., Eds.; Elsevier Science B. V.: Amsterdam, 2000; Vol. *28*, p 53.
(9) Gun'ko, Y. K.; Hitchcock, P. B.; Lappert, M. F. *J. Organomet. Chem.* **1995**, *499*, 213.
(10) Bochkarev, M. N.; Fedushkin, I. L.; Fagin, A. A.; Petrovskaya, T. V.; Ziller, J. W.; Broomhall-Dillard, R. N. R.; Evans, W. J. *Angew. Chem., Int. Ed. Engl.* **1997**, *36*, 133.
(11) Al-Juaid, S.; Gun'ko, Y. K.; Hitchcock, P. B.; Lappert, M. F.; Tian, S. *J. Organomet. Chem.* **1999**, *582*, 143.
(12) Bochkarev, M. N.; Fagin, A. A. *Chem.−Eur. J.* **1999**, *5*, 2990.
(13) Hitchcock, P. B.; Lappert, M. F.; Tian, S. *Organometallics* **2000**, *19*, 3420.
(14) Evans, W. J.; Allen, N. T. *J. Am. Chem. Soc.* **2000**, *122*, 11749.
(15) Bochkarev, M. N.; Fedushkin, I. L.; Dechert, S.; Fagin, A. A.; Schumann, H. *Angew. Chem., Int. Ed.* **2001**, *40*, 3176.
(16) Evans, W. J.; Allen, N. T.; Ziller, J. W. *Angew. Chem., Int. Ed.* **2002**, *41*, 359.
(17) Nief, F.; Turcitu, D.; Ricard, L. *Chem. Commun.* **2002**, 1646.
(18) Jaroschik, F.; Momin, A.; Nief, F.; Le Goff, X.-F.; Deacon, G. B.; Junk, P. C. *Angew. Chem., Int. Ed.* **2009**, *48*, 1117.
(19) Mikheev, N. B.; Auerman, L. N.; Rumer, I. A.; Kamenskaya, A. N.; Kazakevich, M. Z. *Russ. Chem. Rev.* **1992**, *61*, 1805.
(20) Corbett, J. D. *Rev. Chim. Miner.* **1973**, *10*, 239.
(21) Dieke, G. H.; Crosswhite, H. M. *Appl. Opt.* **1963**, *2*, 675.
(22) Martin, W. C.; Zalubas, R.; Hagan, L. *Atomic Energy Levels - The Rare-Earth Elements, the Spectra of La, Ce, Pr, Nd, Pm, Sm, Eu, Gd, Tb, Dy, Ho, Er, Tm, Yb, Lu*; National Bureau of Standards, U. S. Department of Commerce: Washington, D.C., 1978.
(23) Huang, Y.; Freiser, B. S. *J. Am. Chem. Soc.* **1988**, *110*, 4434.
(24) Ranasinghe, Y. A.; MacMahon, T. J.; Freiser, B. S. *J. Am. Chem. Soc.* **1992**, *114*, 9112.
(25) Marçalo, J.; Santos, M.; Pires de Matos, A.; Gibson, J. K.; Haire, R. G. *J. Phys. Chem. A* **2008**, *112*, 12647.
(26) McClure, D. S.; Kiss, Z. *J. Chem. Phys.* **1963**, *39*, 3251.
(27) Mikheev, N. B.; Auerman, L. N.; Rumer, I. A. *Inorg. Chim. Acta* **1985**, *109*, 217.
(28) Mikheev, N. B.; Kamenskaya, A. N. *Coord. Chem. Rev.* **1991**, *109*, 1.
(29) Bond, A. M.; Deacon, G. B.; Newnham, R. H. *Organometallics* **1986**, *5*, 2312.
(30) Evans, W. J.; Lee, D. S.; Lie, C.; Ziller, J. W. *Angew. Chem., Int. Ed.* **2004**, *43*, 5517.
(31) Evans, W. J.; Lee, D. S.; Ziller, J. W. *J. Am. Chem. Soc.* **2004**, *126*, 454.
(32) Evans, W. J.; Lee, D. S.; Rego, D. B.; Perotti, J. M.; Kozimor, S. A.; Moore, E. K.; Ziller, J. W. *J. Am. Chem. Soc.* **2004**, *126*, 14574.
(33) Evans, W. J.; Lee, D. S. *Can. J. Chem.* **2005**, *83*, 375.
(34) Evans, W. J.; Lee, D. S.; Johnston, M. A.; Ziller, J. W. *Organometallics* **2005**, *24*, 6393.
(35) Evans, W. J.; Rego, D. B.; Ziller, J. W. *Inorg. Chem.* **2006**, *45*, 10790.
(36) Evans, W. J.; Fang, M.; Zucchi, G.; Furche, F.; Ziller, J. W.; Hoekstra, R. M.; Zink, J. I. *J. Am. Chem. Soc.* **2009**, *133*, 11195.
(37) Lorenz, S. E.; Schmiege, B. M.; Lee, D. S.; Ziller, J. W.; Evans, W. J. *Inorg. Chem.* **2010**, *49*, 6655.
(38) Schmiege, B. M.; Ziller, J. W.; Evans, W. J. *Inorg. Chem.* **2010**, *49*, 10506.
(39) Demir, S.; Lorenz, S. E.; Fang, M.; Furche, F.; Meyer, G.; Ziller, J. W.; Evans, W. J. *J. Am. Chem. Soc.* **2010**, *132*, 11151.
(40) Fang, M.; Bates, J. E.; Lorenz, S. E.; Lee, D. S.; Rego, D. B.; Ziller, J. W.; Furche, F.; Evans, W. J. *Inorg. Chem.* **2011**, *50*, 1459.
(41) Fang, M.; Lee, D. S.; Ziller, J. W.; Doedens, R. J.; Bates, J. E.; Furche, F.; Evans, W. J. *J. Am. Chem. Soc.* **2011**, *133*, 3784.
(42) Cassani, M. C.; Duncalf, D. J.; Lappert, M. F. *J. Am. Chem. Soc.* **1998**, *120*, 12958.
(43) Hitchcock, P. B.; Lappert, M. F.; Maron, L.; Protchenko, A. V. *Angew. Chem., Int. Ed.* **2008**, *47*, 1488.

(44) Rogers, E.; Dorenbos, P.; van der Kolk, E. *New J. Phys.* **2011**, *13*, 093038.
(45) Taylor, M. D. *Chem. Rev.* **1962**, *62*, 503.
(46) Peterson, J. K.; MacDonald, M. R.; Ziller, J. W.; Evans, W. J. *Organometallics* 2013, ASAP, DOI: 10.1021/om400116d.
(47) Bergbreiter, D. E.; Killough, J. M. *J. Am. Chem. Soc.* **1978**, *100*, 2126.
(48) Golombek, A. P.; Hendrich, M. P. *J. Magn. Reson.* **2003**, *165*, 33.
(49) Dolg, M.; Stoll, H.; Pruess, H. *Theor. Chim. Acta* **1993**, *85*, 441.
(50) Andrae, D.; Haussermann, U.; Dolg, M. *Theor. Chim. Acta* **1990**, *77*, 123.
(51) Weigend, F.; Ahlrichs, R. *Phys. Chem. Chem. Phys.* **2005**, *18*, 3297.
(52) Klamt, A.; Schürmann, G. *J. Chem. Soc., Perkin Trans. 2* **1993**, *5*, 799.
(53) *CRC Handbook of Chemistry and Physics*; 81st ed.; Lide, D. R., Ed.; CRC Press: Boca Raton, 2008; Chapter 8, p 136.
(54) Bauernschmitt, R.; Ahlrichs, R. *J. Chem. Phys.* **1996**, *104*, 9047.
(55) Zirngast, M.; Flörke, U.; Baumgartner, J.; Marschner, C. *Chem. Commun.* **2009**, 5538.
(56) Berthet, J.-C.; Villiers, C.; Le Maréchal, J.-F.; Delavaux-Nicot, B.; Lance, M.; Nierlich, M.; Vigner, J.; Ephritikhine, M. *J. Organomet. Chem.* **1992**, *440*, 53.
(57) Wang, J.-Q.; Fassler, T. F. *Z. Naturforsch., B: J. Chem. Sci.* **2009**, *64*, 985.
(58) Jutzi, P.; Leffers, W.; Hampel, B.; Pohl, S.; Saak, W. *Angew. Chem., Int. Ed. Engl.* **1987**, *26*, 583.
(59) (a) [K(18-crown-6)(toluene)$_2$][Cp″$_3$Sm]: Gun'ko, Y. K.; Hitchcock, P. B.; Lappert, M. F. *Chem. Commun.* **1998**, 1843. (b) [K(18-crown-6)(η^2-toluene)$_2$]{[La(C$_5$H$_4$SiMe$_2$^{t}Bu)$_3$]$_2$(μ-H)} and [K(18-crown-6)(η^2-toluene)$_2$][(CeCp″$_2$)$_2$(μ-η^6:η^6-toluene)]: Gun'ko, Y. K.; Hitchcock, P. B.; Lappert, M. F. *Organometallics* **2000**, *19*, 2832. (c) [K(18-crown-6)(THF)(toluene)]{Ca[N(SiMe$_3$)$_2$]$_3$}: He, X.; Allen, J. F.; Noll, B. C.; Kennedy, A. R.; Henderson, K. W. *J. Am. Chem. Soc.* **2005**, *127*, 6920.
(60) Lehn, J. M. *Struct. Bonding (Berlin)* **1973**, *16*, 1.
(61) Fang, M.; Farnaby, J. H.; Ziller, J. W.; Bates, J. E.; Furche, F.; Evans, W. J. *J. Am. Chem. Soc.* **2012**, *134*, 6064.
(62) Strittmatter, R. J.; Bursten, B. E. *J. Am. Chem. Soc.* **1991**, *113*, 552.
(63) Dolg, M.; Fulde, P.; Stoll, H.; Preuss, H.; Chang, A.; Pitzer, R. M. *Chem. Phys.* **1995**, *195*, 71.
(64) Liu, W.; Dolg, M.; Fulde, P. *Inorg. Chem.* **1998**, *37*, 1067.
(65) Hong, G.; Schautz, F.; Dolg, M. *J. Am. Chem. Soc.* **1999**, *121*, 1502.
(66) Shannon, R. D. *Acta Crystallogr.* **1976**, *A32*, 751.
(67) Evans, W. J.; Foster, S. E. *J. Organomet. Chem.* **1992**, *433*, 79.
(68) Gun'ko, Y. K.; Hitchcock, P. B.; Lappert, M. F. *Chem. Commun.* **1998**, 1843.
(69) Jaroschik, F.; Nief, F.; Le Goff, X.-F.; Ricard, L. *Organometallics* **2007**, *26*, 1123.
(70) For example, Cp$_2$TiCl$_2$: Clearfield, A.; Warner, D. K.; Saldarriaga-Molina, C. H.; Ropal, R.; Bernal, I. *Can. J. Chem.* **1975**, *53*, 1622. [Cp$_2$Ti(μ-Cl)]$_2$: Jungst, R.; Sekutowski, D.; Davis, J.; Luly, M.; Stucky, G. *Inorg. Chem.* **1977**, *16*, 1645. These have average Ti-C(η^5-Cp) bond lengths of 2.370 and 2.350 Å, respectively. Similarly, Cp$_4$Zr: Rogers, R. D.; Bynum, R. V.; Atwood, J. L. *J. Am. Chem. Soc.* **1978**, *100*, 5238. Cp$_3$Zr: Lukens, W. L., Jr.; Andersen, R. A. *Organometallics* **1995**, *14*, 3435. Both have the same average Zr-C(η^5-Cp) bond length of 2.58 Å.
(71) Denning, R. G.; Harmer, J.; Green, J. C.; Irwin, M. *J. Am. Chem. Soc.* **2011**, *133*, 20644.
(72) Bursten, B. E.; Rhodes, L. F.; Strittmatter, R. J. *J. Am. Chem. Soc.* **1989**, *111*, 2756.
(73) Bursten, B. E.; Rhodes, L. F.; Strittmatter, R. J. *J. Am. Chem. Soc.* **1989**, *111*, 2758.
(74) (a) Sattler, J. P.; Nemarich. *J. Phys. Rev. B* **1971**, *4*, 1. (b) Wu, C. Y.; Alben, R.; Wolf, W. P. *Solid State Commun.* **1972**, *11*, 1599. (c) Reynolds, R. W.; Boatner, L. A.; Finch, C. B.; Chatelain, A.; Abraham, M. M. *J. Chem. Phys.* **1972**, *56*, 5607. (d) Kulpa, S. M.; Nemarich, J. *Phys. Lett. A* **1975**, *50*, 461. (e) Ball, D. *Phys. Status Solidi A* **1976**, *35*, 651. (f) O'Connor, C. J.; Carlin, R. L.; Schwartz, R. W. *J. Chem. Soc., Faraday Trans. 2* **1977**, *73*, 361. (g) Spencer, B.; Edelstein, N. M. *Inorg. Chem.* **1981**, *20*, 2736. (h) Fields, R. A.; Hutchison, C. A., Jr. *J. Chem. Phys.* **1985**, *82*, 1711. (i) Baker, J. M.; Hutchison, C. A., Jr.; Martineau, P. M. *Proc. R. Soc. London, Ser. A* **1986**, *403*, 221. (j) Baker, J. M.; Hutchison, C. A., Jr.; Leask, M. J. M.; Martineau, P. M.; Robinson, M. G.; Wells, M. R. *Proc. R. Soc. London, Ser. A* **1987**, *413*, 515. (k) Bellesis, G. H.; Simizu, S.; Friedberg, S. A. *J. Appl. Phys.* **1987**, *61*, 3286. (l) Baker, J. M.; Cook, M. I.; Hutchison, C. A., Jr.; Leask, M. J. M.; Robinson, M. G.; Tronconi, A. L.; Wells, M. R. *Proc. R. Soc. London, Ser. A* **1991**, *434*, 695. (m) Baker, J. M.; Cook, M. I.; Hutchison, C. A., Jr.; Martineau, P. M.; Tronconi, A. L.; Weber, R. T. *Proc. R. Soc. London, Ser. A* **1991**, *434*, 707. (n) Klein, P. B.; Moore, F. G.; Dietrich, H. B. *Appl. Phys. Lett.* **1991**, *58*, 502. (o) Milori, D. M. B. P.; Hernandes, A. C.; de Souza, R. R.; Siu, Li, M.; Terrile, M. C. *Phys. Rev. B* **1995**, *51*, 3206. (p) Baker, J. M.; Hutchison, C. A., Jr.; Jenkins, A. A.; Tronconi, A. L. *Proc. R. Soc. London, Ser. A* **1997**, *453*, 417. (q) Tarasov, V. F.; Shakurov, G. S.; Malkin, B. Z.; Hutchison, C. A., Jr. *J. Alloys Compd.* **1997**, *250*, 364. (r) Asatryan, H. R.; Rosa, J.; Mareš, J. A. *Solid State Commun.* **1997**, *104*, 5. (s) Dunbar, T. D.; Warren, W. L.; Tuttle, B. A.; Randall, C. A.; Tsur, Y. *J. Phys. Chem. B* **2004**, *108*, 908. (t) Konovalov, A. A.; Lis, D. A.; Malkin, B. Z.; Nikitin, S. I.; Subbotin, K. A.; Tarasov, V. F.; Vorobieva, E. N.; Zharikov, E. V.; Zverev, D. G. *Appl. Magn. Reson.* **2005**, *28*, 267.
(75) Cotton, S. *Lanthanide and Actinide Chemistry*; John Wiley & Sons Ltd.: West Sussex, 2006.
(76) Symons, M. C. R.; Baker, J. M. In *Electron Spin Resonance*; Symons, M. C. R., Ed.; Royal Society of Chemistry: Cambridge1993; Vol. *13B*, p 131.
(77) Anderson, D. M.; Cloke, F. G. N.; Cox, P. A.; Edelstein, N.; Green, J. C.; Pang, T.; Sameh, A. A.; Shalimoff, G. *J. Chem. Soc., Chem. Commun.* **1989**, 53.
(78) Knapp, C.; Weiden, N.; Dinse, K.-P. *Appl. Phys. A: Mater. Sci. Process.* **1998**, *66*, 249.
(79) In simple isotropic $S = 1/2$ systems with hyperfine coupling to one atom of nuclear spin, I, the first-order perturbation equation for EPR transition energies is: $h\nu = g\beta H + Am_I$ (h = Planck constant; ν = frequency of radiation; g = spectroscopic splitting factor; β = Bohr magneton; H = magnetic field strength; A = hyperfine coupling constant; m_I = nuclear spin angular momentum quantum number). This equation assumes that $h\nu \gg A$, which does not hold true for **4-Lu**. A second-order perturbation term must be incorporated in this case: $h\nu = g\beta H + Am_I + A^2[I(I+1) - m_I^2]/(2g\beta H)$.[80]
(80) Rieger, P. H. *Electron Spin Resonance: Analysis and Interpretation*; The Royal Society of Chemistry: Cambridge, 2007.
(81) Evans, W. J.; Grate, J. W.; Choi, H. W.; Bloom, I.; Hunter, W. E.; Atwood, J. L. *J. Am. Chem. Soc.* **1985**, *107*, 941.
(82) Evans, W. J.; Ulibarri, T. A.; Chamberlain, L. R.; Ziller, J. W.; Alvarez, D., Jr. *Organometallics* **1990**, *9*, 2124.
(83) Cloke, F. G. N. *Chem. Soc. Rev.* **1993**, *22*, 17.
(84) King, W. A.; Di Bella, S.; Lanza, G.; Khan, K.; Duncalf, D. J.; Cloke, F. G. N.; Fragala, I. L.; Marks, T. J. *J. Am. Chem. Soc.* **1996**, *118*, 627.
(85) Brewer, L. In *Systematics and the Properties of the Lanthanides*; Sinha, S. P., Ed.; Reidel: Dordrecht, 1983, p 17.
(86) Dorenbos, P. *J. Phys.: Condens. Matter* **2003**, *15*, 575 and references therein.